WEIZMANN INSTITUTE OF SCIENCE

Thesis for the degree
Doctor of Philosophy

By
Yoav Gordin

חבור לשם קבלת התואר
דוקטור לפילוסופיה

מאת
יואב גורדין

מדידת תכונות הולכה של מולקולות אורגניות בודדות בעזרת
ננו-חלקיקים מזהב

Measurement of the conductance properties of single organic molecules using gold nanoparticles

Regular Format

Advisors
Prof. Israel Bar-Joseph
Prof. Amir Yacoby

מנחים
פרופ. ישראל בר-יוסף
פרופ. עמיר יעקבי

December 2006

דצמבר 2006

UMI Number: DP17870

INFORMATION TO USERS

The quality of this reproduction is dependent upon the quality of the copy submitted. Broken or indistinct print, colored or poor quality illustrations and photographs, print bleed-through, substandard margins, and improper alignment can adversely affect reproduction.

In the unlikely event that the author did not send a complete manuscript and there are missing pages, these will be noted. Also, if unauthorized copyright material had to be removed, a note will indicate the deletion.

UMI®

Acknowledgements

Abstract

In this work we describe the development and application of a new method for the electrical conductance measurement of single molecules. The study of single molecule conductance is a young field with many open questions. The issue of reliable theoretical modeling of molecular electronic transport is still very much in debate, with significant discrepancies between theoretical predictions and experiment. The experimental methods used in the field are very difficult to realize and interpret; most have very low yield, preventing proper statistical analysis and many have problems in the researchers' ability to characterize the system properly.

We address this issue by using self assembly of gold nanoparticle-molecule-gold nanoparticle objects called dimers. This method allows fabrication of molecular junctions with greater ease; moreover it allows individual characterization of the various elements of the junction, removing much of the uncertainties that exist in this kind of measurements. We make use of home grown gold nanoparticles with a few tens of nanometer diameter to form the hybrid dimers. The dimers are large enough to connect between electrodes fabricated using electron beam lithography and to measure the electric properties of the molecule. We have invested significant effort in the characterization of the system, ensuring that the dimers are indeed bridged by the molecules, and that the chances that more than a single molecule exists in a dimer are negligibly small.

We have made measurements on single gold nanoparticles, to characterize their properties separately from those of the molecule. These measurements have allowed us to observe single electron transistor (SET) behavior, resulting from the requirement that electrons charge the nanoparticle during transport. We have shown that the energy associated with this charging scales with nanoparticle size as expected.

We have performed measurements on single organic molecules, showing that there is a very strong influence of molecular conjugation (the way electronic orbitals are spread along the molecular backbone) on its conductance. The molecules with broken conjugation conduct more than an order of magnitude less than those that are fully conjugated.

A distinct feature of the conjugated molecule is the appearance of pronounced peaks in its conductance at certain voltage values. We have shown that these peaks can be gated randomly by the electrostatic environment, but the peak spectrum is

reproducible among the different samples of the same molecular species that we studied.

To properly study and understand the peak structure we developed the ability to add gate dependent measurements to our system. Unfortunately the backdrop of this was a drastic reduction in the yield of good samples for measurement. We focused on four different conjugated molecules to attempt to understand the effect of the molecular structure on the properties of the peak spectra. We have been able to measure three of these molecules, and obtained SET diamond plots reminiscent of those seen for the single particles. The molecular diamonds have a larger energy gap than that found in single particles, as can be expected from their smaller size. We do not yet have enough data on this issue to make any definite statements on the influence of the molecular structure on the peak structure.

Another topic investigated in this work is the physics of the two gold nanoparticles, giving rise to double quantum dot (DQD) phenomena. This physics is observed in dimers that do not exhibit "molecular" (high energy) features, or at low voltages before the appearance of the molecular peaks. We have used these phenomena to fully characterize the properties of our system and understand better the role the molecule plays in transport at low bias (below the voltage of the first peak).

I begin this thesis with an introduction to the field of molecular electronics; I briefly review the theoretical approaches and the experimental methods used. I then describe in detail the dimer method, whose development took up a major part of this work, relaying in detail the relevant issues and considerations. I relate briefly some early measurements done on single nanoparticles to verify our understanding of transport in the system. Moving to the description of single molecule conductance measurements I start by describing measurements demonstrating the importance of conjugation to molecular conductance. I discuss in detail the peaks appearing in the conductance measurements of the conjugated molecules describing their sample to sample variability, temporal behavior and temperature dependence. I describe the importance of gating for a comprehensive understanding of the peak spectrum and present some preliminary measurements of three different molecular species that we have been able to gate. In the final chapter of this work I describe the double quantum dot phenomena observed in the dimer system; these phenomena are not immediately relevant to the issue of single molecule conductance, but serve as a tool to characterize our system fully while providing assurance that the current goes through both nanoparticles.

תקציר

בתזה זו אנו מתארים את הפיתוח והיישום של שיטה חדשה למדידת תכונות ההולכה של מולקולות בודדות. המחקר של הולכה במולקולות בודדות הוא תחום צעיר בעל שאלות פתוחות רבות. הנושא של תיאור תיאורטי אמין של הולכה חשמלית במולקולות עדיין נתון לויכוח, כאשר יש חוסר התאמה משמעותית בין תחזיות תיאורטיות ונסיון. השיטות הנסיוניות הקיימות בשטה הן מאד קשות ליישום ולהבנה: לרובן אחוז הצלחה נמוכים מאד. המונעים אנליזה סטטיסטית של התוצאות ולרבות מהן יש בעיות ביכולת החוקרים לאפיין ולתאר את המערכת באופן מלא.

אנו מתמודדים עם הנושא על ידי שימוש בשיטה של הרכבה עצמית (self assembly) של אובייקטים בעלי מבנה של ננו הלקיק מזהב-מולקולה-ננו הלקיק מזהב המכונים דימרים. שיטה זו מאפשרת יצירת צמתים מולקולריים בקלות יחסית; יתרה מכך היא מאפשרת אפיון בנפרד של רכיבי הצומת השונים, ובכך מסירה הרבה מאי הוודאות הקיימת במדידות מסוג זה. אנו עושים שימוש בבנו חלקיקים מזהב בעלי קוטר של כמה עשרות ננומטרים לייצור הדימרים. הדימרים גדולים מספיק בשביל לגשר בין אלקטרודות המיוצרות באמצעות ליתוגרפיה בקרן אלקטרונים על מנת למדוד את ההולכה החשמלית דרך המולקולה. השקענו מאמץ ניכר באפיון המערכת. וידוא שהדימרים אכן מגושרים על ידי המולקולה ושהסיכוי לקיום יותר ממולקולה אחת בדימר הוא קטן במידה זניחה.

בצענו מדידות של חלקיקי זהב בודדים , על מנת לאפיין את תכונותיהם בנפרד מהמולקולה. מדידות אלו אפשרו לנו למדוד התנהגות של טרנזיסטור של אלקטרון בודד (single electron transistor), הנובעות מהצורך לטעון את ההלקיק במהלך העברת הזרם. הראינו שסקאלות האנרגיה הקשורות לטעינה זו משתנות בהתאם לגודל ההלקיק כצפוי.

בצענו מדידות על מולקולות אורגניות והראינו שיש השפעה חזקה למידת הצימוד האלקטרוני (conjugation) (הפריסה של המצבים האלקטרוניים לאורך המולקולה) של המולקולה על המוליכות שלה. המוליכות של מולקולות שבהן הצימוד האלקטרוני נשבר נמוכה בלמעלה מסדר גודל ביחס למולקולות שיש בהן צימוד טוב.

תכונה בולטת של המולקולות המצומדות היא הופעה של שיאים בולטים בערכי מתח מסוימים. הראינו ששיאים אלה יכולים להיות מוסטים חשמלית באופן רנדומי על ידי הסביבה האלקטרוסטטית אך הספקטרום שלהם הוא די הדיר עד כדי הזזה בין דוגמאות שונות שמכילות את אותו סוג של מולקולה.

לשם לימוד מלא של מבנה השיאים של המולקולה פיתחנו את היכולת לשלוט אלקטרוסטטית ברמות האנרגיה של המולקולה (gating). לרוע המזל החסרון בכך היה בהורדה משמעותית של התפוקה של דוגמאות טובות למדידה. התמקדנו בארבעה סוגים שונים של מולקולות מצומדות, בנסיון להבין את הקשר בין מבנה המולקולה לתכונות ספקטרום השיאים שלה. הצלחנו למדוד שלושה סוגי מולקולות שונים מהסוגים שהתמקדנו בהם ולקבל דיאגרמות יהלום דומות לאלו המתקבלות עבור טרנזיסטור של אלקטרון בודד. היהלומים המולקולריים הם בעלי פער אנרגיה גדול יותר מזה שמתקבל בהלקיקים בודדים. כפי שניתן לצפות מגודלן הקטן יותר. עדיין אין בידינו די מידע על מנת לומר הצהרות נחרצות כלשהן לגבי ההשפעה של מבנה מולקולרי על ספקטרום ההולכה.

נושא נוסף שעלה בעבודה זו הוא הפיזיקה של שני כדורי הזהב. שיוצרים התנהגות של נקודות קוונטיות כפולות (double quantum dots). פיזיקה זו נצפית בעיקר בדימרים שבהם אין הופעה של שיאים "מולקולריים" (באנרגיות גבוהות) או במתחים נמוכים, לפני הופעת השיא המולקולרי הראשון.

7

השתמשנו בתופעות אלה כדי לאפיין את תכונות המערכת שלנו באופן מלא ולהבין טוב יותר את התפקיד שממלאת במולקולה בהולכה במתח נמוך (לפני הופעת השיא הראשון).

אני מתחיל תזה זו בהקדמה לתחום האלקטרוניקה המולקולרית. אני מתאר בקצרה את הגישות התיאורטיות ואת השיטות הניסיוניות הקיימות. אחר כך אני מתאר בפירוט את שיטת הדימרים. שפיתוחה היווה חלק משמעותי מעבודה זו, ומתעכב על השיקולים השונים הרלוונטיים להבנת השיטה. אני מתאר בקצרה מדידות מוקדמות שביצענו על ננוחלקיקים בודדים על מנת לוודא את הבנתנו לגבי ההולכה במערכת. בתאור העבודה שנעשתה לגבי הולכה במולקולות בודדות אני מתחיל במדידות שביצענו על החשיבות של הצימוד האלקטרוני להולכה המולקולרית. אני דן בפירוט בשיאים המופיעים במדידות ההולכה של מולקולות מצומדות ומתאר את השתנותם מדגם לדגם. התנהגותם התלויה בזמן והשפעת הטמפרטורה עליהם. אני דן בחשיבות היכולת לשלוט בהולכה ע"י אלקטרודת "שער" (gate) על מנת להבין באופן מלא את ספקטרום השיאים ומציג מספר תוצאות ראשוניות של מדידות על שלושה סוגי מולקולות שונים. בפרק האחרון של העבודה אני מתאר את התופעות הקשורות לשתי נקודות קוונטיות שהתגלו במערכת הדימרים. תופעות אלו אינן קשורות ישירות לנושא ההולכה המולקולרית, אך הן משמשות ככלי לאפיון מלא של המערכת וכן לאישוש ההנחה שהזרם עובר דרך שני החלקיקים.

Contents

Scientific background

Over the past years there has been great scientific interest and effort invested in the field of nanotechnology and more specifically in single molecule based technology. The ongoing trend of miniaturization in electronic circuits has led many people to conclude that within several years the typical scale of electronic components will approach the molecular scale. Besides the obvious advantage of increased miniaturization the possibility of creating materials and structures from their basic building blocks can allow better control of their properties; it also opens the possibility of manufacturing structures using the "bottom up" approach, which makes use of chemical reactions to produce many complex structures in parallel. Thus nanotechnology is not only a natural extension of the trends existing today in the industry, it is also an opening to an entirely new approach towards material science and engineering.

An important property of molecules that needs to be understood if we are to make use of them in nanoelectronics is that of their electrical behavior. Understanding the way molecular structure affects the electrical transport properties of single molecules can enable us to design and manufacture molecules for specific electrical components, paving the way towards molecular electric circuits, and perhaps molecular computers. Since Aviram and Ratner [1] first proposed the possibility of creating rectifiers based on single molecules in 1974, much scientific effort has been invested in the realization of molecule based electronic components. Primarily research effort was put mostly in the measurement of electron transport rates through a molecular bridge between two molecular redox centers. In this method one places a molecular bridge between a donor site, This approach has allowed researchers to observe various transport phenomena in molecules, such as molecular wires (i.e. molecules whose transmission depends very weakly on length) [2,3], molecules that display structural changes and, thus, electrical switching upon exposure to light [4], and molecules that display interference effects in their transport behavior [5]. The quantity measured here is not conductance, but rather the rate of electron transfer through the molecular bridge; the relationship between the electron transfer rate $K_{D \rightarrow A}$ and the molecular conductance g of metal-molecule-metal junctions has been worked out by Nitzan [6], it is given by

the equation $g \sim \dfrac{8e^2}{\pi^2 \Gamma_D^{(L)} \Gamma_A^{(R)} F} K_{D,A}$ with F the thermally averaged and Franck-Condon weighted density of nuclear states, e is the electron charge, and Γ the coupling to the left or right leads. While this approach has served to improve understanding of the factors influencing charge flow through molecules, it is clearly less relevant for device applications. The correspondence between the properties of free molecules and ones which are bonded to metallic surfaces is also not clear, the effect of image charges in the metal, for example, is not taken into account in the above calculation.

Much of the insight and understanding in molecular electronics has been gained by measurement of the conduction properties, not of single molecules, but of self assembled monolayers (SAMs) of molecules. This approach has led to a better understanding of the processes involving charge transfer through molecules, and the effect of the contact to the substrate [7], but in many of these cases it has been observed that the transport is affected by the intermolecular interactions inside the monolayer and therefore these results are not immediately applicable to the behavior of single molecule junctions. The study of single molecule electronics has gained significant advances over the past years allowing researchers to better study the properties of single molecules and several reviews have been written on this topic [8,9,10]

Theoretical approaches

The single electron transistor

The description of transport through zero dimensional systems, such as depicted in figure 1 is done using the formalism of single electron tunneling [11]. This formalism is too simplistic to describe molecular conductance, since it

Figure 1 – Schematic illustration of an SET circuit. Illustration of a system showing SET behavior, electrons need to tunnel from the leads to the dot for transport to occur.

does not include any information on the chemical properties of the molecule, but it is helpful in gaining insight to the issues influencing charge transport through low dimensional systems. The physics of single charge tunneling describes very well the mechanism of charge transport through the gold nanoparticles and is therefore also
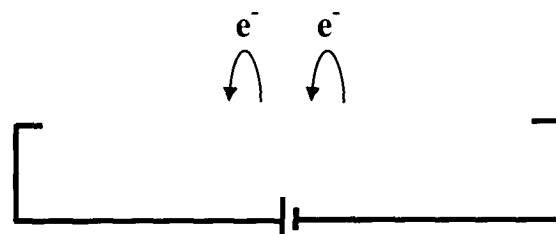
necessary for a complete description of the dimer system as we shall show later in this work. The electrostatic energy of a metal island as a function of its charge is given by $E=Q^2/2C_\Sigma-QV_g$, where Q is the charge on the island, C_Σ the total capacitance of the island to both leads and to the gate, and V_g the gate voltage. This energy is minimized by a charge $Q_0=C_\Sigma V_g$ which in principle is a continuous function of V_g. The discreteness of the electric charge, however, implies that the island can be charged only by an integer number of electrons. In order to transfer current through the island it is necessary for an electron to be able to tunnel in and out of it. This condition is met only when the energy of the dot charged by N electrons is equal to that of N+1 (figure 2b). If this condition isn't fulfilled (e.g. figure 2a) current is blocked at low bias. In this case current will flow only for a source drain voltage between the electrodes that exceeds the charging energy $V_{sd}\geq e/2C_\Sigma$. The current voltage characteristic of the system will thus exhibit a gap prohibiting current near zero bias, known as the Coulomb blockade (CB). Scanning the gate voltage will allow us to shift the parabola causing the energy gap from N to N+1 to diminish gradually, once we reach the state $Q_0=(N+1/2)e$ the two states with N and N+1 electrons become degenerate, closing the gap, and current can flow through the system at infinitesimal bias (figure 2b). It is easy to see that this behavior will be periodic in V_g, switching from an island ground state with N electrons to N+1, N+2, etc. In source drain voltage scans there will be a conductance peak when the energy supplied by the voltage equals the energy required to add further electrons to the dot. If there is an asymmetry between the two tunnel junctions connecting the island and the leads there is a different rate for electrons entering and leaving the dot; this leads to the appearance of further peaks corresponding to energies of more electrons in the dot and we get the phenomena of the "Coulomb staircase" [11]. Creating a plot of the conductance as function of source drain and gate voltage shows the opening and closing of the source drain gap by the gate yielding the CB diamond plot (figure 2c).
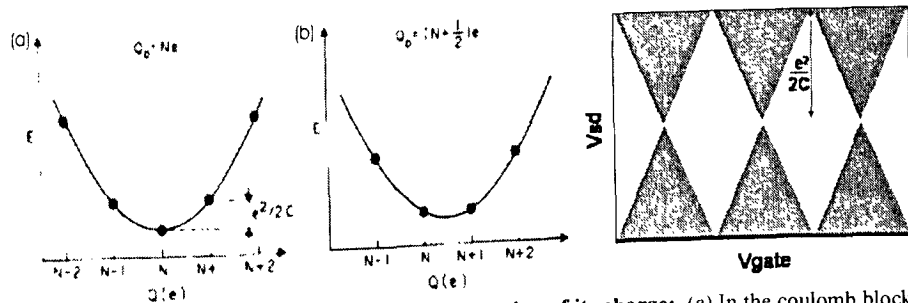

Figure 2 - The energy of an SET island as a function of its charge: (a) In the coulomb blockade region there is a gap of size $e^2/2C_\Sigma$ for charge transport through the island (b) Changing gate voltage shifts the parabola allowing charge to flow freely. (c) Illustration of the CB diamond plot.

Molecular conductance

The theoretical description of transport through a molecular junction is in many ways reminiscent to that of a quantum dot. The electron can pass through the molecule only if it has enough energy to go through an energy level of the molecule. Thus the problem of molecular conductivity is solving the energy levels of the molecule when it is connected to the metallic leads, to find at which source drain voltage values it will conduct. A full description of the methods and approaches used in solving this problem is beyond the scope of this work, but I will try to give a brief overview of the principles, focusing mostly on the method of density functional theory, which is very commonly used in the field. For more elaborate reviews of the topic, see reference [12] and references therein.

To calculate the electrical conductance of molecular systems one may use the Landauer formalism [13]. This approach treats the transport as an elastic single electron process, with the molecule serving as a scattering center. In the Landauer formalism the current through a molecular junction at applied source drain voltage V_{sd}

is given by $I = \frac{e^2}{\pi\hbar} \int_{-\infty}^{\infty} T(E, V_{sd})[f(E) - f(E - eV_{sd})]dE$ where e is the electron charge,

$\hbar$ is the Planck constant multiplied by 2π, $T(E, V_{sd})$ is the transmission coefficient of the molecule, and f is the Fermi distribution of the electrodes given by

$f = [1 + \exp(\frac{E - E_f}{K_B T})]^{-1}$. The transmission function is dependent on the externally

applied bias voltage V_{sd} due to the electrostatic effect it has on the molecular orbitals. The main challenge in the molecular transport problem is the correct calculation of the transmission function for each specific case. The system is usually divided into two semi-infinite leads that serve as electron reservoirs, and the extended molecule, which is comprised of the molecule, and a few atomic layers of the metallic leads. The extended molecule is treated as the part of the system in which the entire scattering takes place; it is chosen so that it encloses an area of the system that maintains electric neutrality.

The simplest approach to calculating the energy spectrum of the molecule is based on a tight binding–type one-electron picture. As illustrated in figure 3b, the structures on the left and on the right are the metal electrodes, and the atomic basis functions within the molecule are represented by line segments [15]. There can be interactions among

the atomic levels, and any of them can couple to the electrode. More commonly, one thinks of the molecular orbitals of the molecule within the junction. Allowing interaction between the molecule and the metal electrodes indicated in figure 3a, some charge flow, charge rearrangement, and geometric reorganization will occur. One can simplify this viewpoint by expressing the system by the level scheme depicted in figure 3b. Here the Fermi level of the electrodes lies within the HOMO-LUMO (Highest Occupied Molecular Orbital - Lowest Unoccupied Molecular Orbital) gap of the molecule. This picture is oversimplified, assuming that mixing between a molecule and an electrodes is relatively weak compared with the interatomic interactions that give rise to the molecular electronic structure.
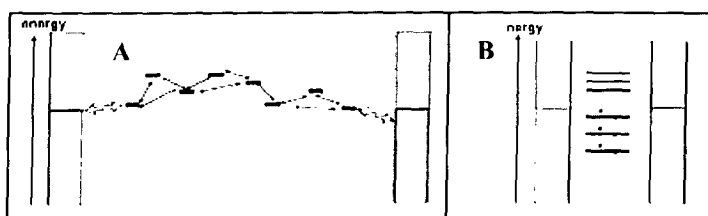
Figure 3: Schematic description of molecular conductance.

(a) Illustration of a molecular wire, striped arrows indicate coupling between molecular levels and electrode and black arrows indicate intersite interactions along the molecular chain. The filled and empty parts of the rectangles represent filled and empty levels of the electrode conduction bands (b) Molecular orbitals. Electrode Fermi level lies in the HOMO-LUMO gap. [15]

The energy dependence of the molecular transmission function stems directly from the density of states of the extended molecule. It is essentially given by the source and drain couplings (which may themselves have an energy dependence) multiplied by the molecular density of states. When the molecule is connected to metallic leads there is hybridization between the states of the molecule and the density of states of the leads. This will typically lead to a broadening of the molecular energy levels and also to the appearance of new states in the energies that were previously in the molecular energy gap. The exact way in which this hybridization will change the energy spectrum will depend on the specific properties of the leads and on the type of connection between the molecule and the leads. Calculation of this change in the molecular spectrum is the main challenge of the theoretical work done in this field.

To properly calculate the actual current voltage characteristics of a specific molecular junction one needs to calculate the molecule transmission function taking into account

the specific atomic degrees of freedom of the molecule being used, as well as the exact configuration of the connection to the leads. To solve this problem precisely one needs to solve the many body Schrödinger equation of the junction including electron-electron interactions. An exact solution to this problem is not possible except for cases where there is only one electron in the system, thus making it necessary to make some approximation, reducing the many body problem to a solvable model. This is usually done using density functional theory (DFT). In this method the electrons are described as non-interacting particles moving in an effective potential set up by the other electrons. The effective potential depends on the average position of the other electrons, and needs to be determined self-consistently. The general algorithm for DFT calculations is as follows:

1) $H_{1el} = -\dfrac{\hbar}{2m}\nabla^2 - V^{eff}[n](r)$.

2) $H_{1el}\Psi_\alpha(r) = \varepsilon_\alpha \Psi_\alpha(r)$.

3) $n(r) = \displaystyle\sum_{\varepsilon \leq \mu}\Psi_\alpha(r)$.
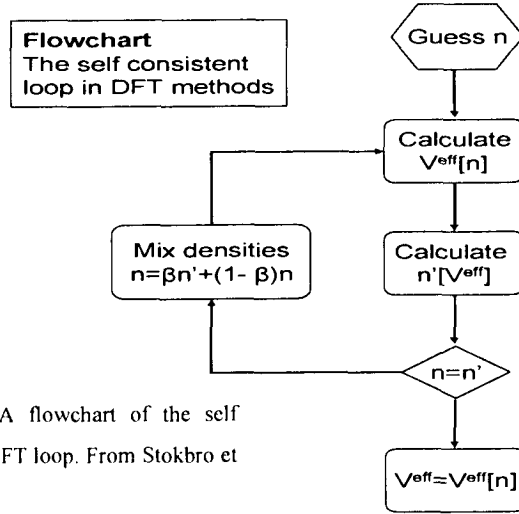
Figure 4: A flowchart of the self consistent DFT loop. From Stokbro et al. ref 11.

The first equation defines the one-electron Hamiltonian, where $\dfrac{\hbar}{2m}\nabla^2$ describes the kinetic energy and $V^{eff}[n](r)$ the effective potential energy of the electron in the extended molecule. The effective potential depends on the electron density, n. From the one-electron Hamiltonian one can determine the eigenstates by solving the Schrödinger equation 2. The electron density is determined by summing all occupied eigenstates, i.e. states with an energy below the chemical potential of the system, μ. The flowchart in figure 4 illustrates the self-consistent loop required to solve the equations.

Solving the equations of the DFT method is usually done by making use of the non equilibrium Greens function (NEGF) formalism. The full description of the NEGF method is beyond the scope of this introduction, but I will endeavor to give a brief

overview. In the NEGF one calculates the charge density from the Greens function of the molecular junction. After separating the system into two semi infinite leads and an interaction region (the molecule and several layers of atoms in the leads) one studies each subsystem separately. The Greens function of the interaction region is found by treating the interaction with the leads as a perturbation, while the lead Greens function is found by recursive methods relying on their being periodic structures. The transmission of the molecular junction is found from the Greens function through the equation:

$$T(\varepsilon) = Tr[\operatorname{Im}\hat{\Sigma}_L(\varepsilon)\hat{G}(\varepsilon)\operatorname{Im}\hat{\Sigma}_R(\varepsilon)\hat{G}(\varepsilon)] \quad [16].$$

The use of DFT type calculations is very widespread in the field of molecular electronics allowing study of the many basic questions. These methods were used to study the alignment of the molecular orbitals with the electrode energy bands [17], demonstrate the influence of end groups on the molecular conductance [18] and study the nonequilibrium electron distribution under applied bias [19]. While they have served to elucidate some of the important questions in the field, this widespread use is problematic. The DFT calculation is a mean field theory; it is therefore applicable only in cases where electron-electron correlations do not play an important role. It will be applicable if the connection of the molecule to the leads is good, that is if the charging energy of the molecule is larger than the molecule electrode coupling. In the Coulomb blockade limit, where the connection is essentially through a tunnel barrier, it will no longer apply. In the case of small molecules , such as the ones studied in this work the charging energy is expected to be in the eV range, while the coupling is usually estimated at < 0.2 eV. Thus to study such molecules one needs a different formalism. This can be seen in the recent paper by Lindsay and Ratner [20] comparing measurements and DFT calculation, where the worst fit can be seen for the small conjugated molecules.

In a recent paper Datta and coworkers [21] have proposed a new formalism termed configuration interaction (CI) for calculation of molecular conductance in the CB regime. In this formalism transport occurs at transitions between ground states of the molecule with different electron numbers, while the leads are treated as perturbations using the molecule-lead couplings as fitting parameters. The quantities used in the CI method are $2^N \times 2^N$ matrices, with N the number of single particle basis sets used, allowing accurate treatment of strong interactions. The CI method is used in the paper

to analyze experiments performed on benzene di thiol molecules, with a reasonably good fit. Unfortunately due to the large size of the matrices used in the calculation using it for larger molecules is difficult and will probably require more theoretical work. The CI formalism is quite new, and needs to be examined further before one can make any clear statements on its usefulness, but it is an important attempt to address the problems of DFT type calculations in the molecular electronics field.

Experimental work on molecular conductance

Experimental study of molecular conductance is a very difficult challenge. The technological problem of creating closely spaced electrodes, which can be bridged by a molecule, is a formidable one. In the early stages of the development of the field the main goal of the experimental work done was to demonstrate the possibility of molecular electric transport measurements. Several methods were used to form molecular sized gaps between two electrodes (these methods will be presented in the following chapter), molecules were placed in the gap and conductance was measured. The main challenge was finding a signature of the molecules that will prove that the current is indeed going through them. Some examples of such measurements are the connection between measurement of symmetric/antisymmetric molecules and the correspondence with symmetric/ antisymmetric I-V curves [22] and very notably the observation of the Kondo effect in spin polarized molecules [23]. In parallel there was a continued search for interesting new functionalities in molecular junctions, such as negative differential resistance [24]. More physical understanding could be found in measurements performed on larger molecules such as C60, where researchers where able to observe and identify the electronic spectrum of the molecule [25], and also to demonstrate a correspondence between molecular deformation and amplification of its conductance [26]. A major problem that hounded the field was the irreproducibility of results; the same molecules measured using different methods could yield very different results [8]. A significant breakthrough in the field was the emergence of the conductance histogram method. This method will be elaborated upon in the next chapter where we will discuss different methods for molecular conductance. In brief it is based on repeated creation of many thousands of molecular junctions and measuring their low voltage conductance. This method created a statistically well defined way to measure the low voltage conductance of a single molecule, thus allowing for the first fully characterized molecular junction, that of an H_2 molecule on platinum electrodes.

Measurement of H_2 on Pt electrodes

A significant movement towards more statistically reliable data was achieved with the introduction of the conductance histogram method [27], which will be described in more detail in the next section. This method provides much larger data sets and thus enabled researchers to measure the conductance of an H_2 molecule on Pt leads, demonstrating a conductance of $1G_0$ ($G_0 = 2e^2/h$) (Figure 5a). Studying the conductance fluctuations showed a clear suppression at the value of $1G_0$ indicating a single channel with a transmission close to 1. The system of H_2 on Pt was studied theoretically using the DFT method [28] and the results of the measurement were reproduced; it was shown that the conduction channel arises from a hybridization of the antibonding electron state of
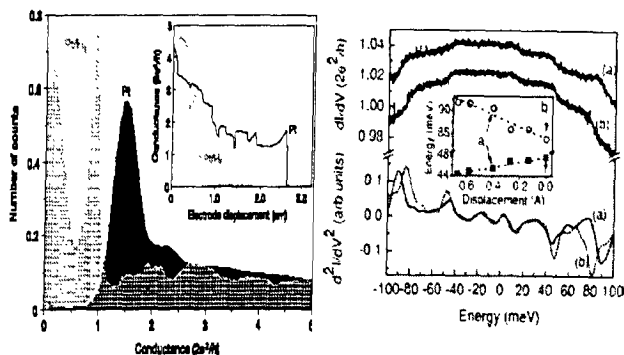
Figure 5: Measurements of the H_2 on Pt system. (a) Histograms of a Clean Pt wire (in black, with 10mV bias) and with an H_2 atmosphere (in grey, with 140mV bias) showing the clear peak at $1G_0$. The inset shows typical breaking curves. (From 27) (b) Peaks in the current second derivative before (curve a) and after (curve b) stretching the junction by 0.04 nm. The peak at ~-90 mV rises in energy, while that at ~-45mV is decreased (From29).

the H_2 with the bands of the Pt leads. The researchers were also able to study the peaks found in the second derivative of the current and observe that replacing the Hydrogen atoms with Deuterium caused them to shift to a lower energy, indicating that the peaks are a result of the vibrations of the H_2 molecule. Studying the dependence of the peaks on stretching of the molecular junction [29] showed that some rose in energy when the molecule was stretched, while others had reduced energy (figure 5b). This allowed assignment of these peaks to transverse and longitudinal modes correspondingly.

This system of the H_2 molecule sandwiched between Pt leads was the first to be fully characterized and understood, both thanks to the new measurement method and due to the simplicity of the system.

Study of more complicated molecules was still not well understood and difficult to explain fully, due to the difficulty in theoretical modeling of such systems. One could, however study the effect of various parameters on the transport through more

complex molecules, and thus gain better understanding of the processes involved.

Effect of molecule length

When studying molecular electronic properties, one of the first issues that need to be addressed is that of the dependence of the molecular conductivity on the length of the molecule. A goal that has taken much effort in the recent years is that of obtaining a "molecular wire", that is a molecular that is able to transport charge efficiently over a significant length. The study of wire shaped molecules has focused on two classes of molecular wires to date: saturated and conjugated molecules.

A class of molecules that has been extensively studied is that of alkane chains [8]; these consist of saturated C-C bonds terminated by linkers that bind to the metallic electrodes. These molecules have large HOMO-LUMO gaps typically on the scale of 7-9 eV, and are considered poor conductors; however due to the ability to synthesize them at any desired length they have become a model system to test the various techniques of molecular electronics. The experiments performed on alkane chains have shown that their conductance (G) decreases exponentially with length (L), showing a tunneling dependence of the kind $G = A\exp(-\beta L)$, where A is a constant, that varies among the different experiments, due to different geometries or differences in the number of molecules measured, and β a constant varying between 0.7-0.9 Å^{-1}.

While alkanes have provided a good testing ground for the different approaches toward molecular electronics, they clearly cannot serve as wires. Better candidates for long conducting molecules are conjugated molecules; these molecules consist of alternating double and single bonds between the carbon atoms that comprise them, leading to a delocalization of their π electrons. These molecules have smaller HOMO-LUMO gaps of 3-5 eV, and thus should be more effective conductors. They were studied at first using systems with molecules bridging donor and acceptor sites [30] or a redox site and a bulk electrode [31], showing that they allow conduction over longer distances than alkane chains and that at longer distances there is a crossover from tunneling to a hopping regime. Corroborating these results with those of metal-molecule-metal junctions is difficult due to the difficult fabrication and low yield of these measurements. A measurement performed on carotenoid polyenes using a statistical analysis approach [32] (See next section) yielded a β of 0.22±0.4 Å^{-1} demonstrating the ability of these molecules to conduct over longer distances. However the behavior of conjugated molecules is more complicated as can be seen

for example for oligothyophenes, where a comparison was made between molecules with three and four repeating units, finding a larger conductance in the longer molecule [33]. This was explained by a smaller HOMO-LUMO gap in the longer molecule, and a closer alignment of the HOMO to the electrode Fermi energy.

Temperature dependence

Direct tunneling is only one option for current to flow through a molecular junction; charge transport through a molecule can also occur through thermally activated hopping, in this mechanism the electron passes through several sites on the molecule, dwelling for a short while in each. This necessarily entails changes in the molecule itself to accommodate the charging of these molecular sites, and therefore will be possible if there is a relevant vibrational mode that enables the electron to hop on to the molecule. The vibrational mode should have an energy within a few $K_B T$ of the lead energy, so that it will be accessible to the transport electrons. Since this transport mechanism is thermally activated the conductance will have a clear exponential dependence on temperature, of the kind $G \sim \exp(-\Delta E / K_B T)$. The length dependence of thermally activated hopping is much weaker than that found in direct tunneling; the current flow is essentially diffusion in one dimension, leading to a logarithmic dependence on the number of molecular sites.

Current through molecules is comprised of contributions from both mechanisms, if the molecule has only one state at an energy ΔE above E_F the low bias conductance can be expressed as:

$$g(E_F) = \frac{e^2}{\pi \hbar} T_{el}(E_F)[1 + (1 - f(E_F + \Delta E)) \frac{\kappa}{\Gamma} \exp(\frac{-\Delta E}{KT})] \quad [34]$$ where T_{el} is the elastic

transmission through the molecule, Γ the imaginary part of the self energy associated with the interaction of the molecular state with the metal electrodes, and κ is a parameter giving the strength of the

Figure 6: Arrhenius plots of an OPE molecule (shown on right) junction. The set of curves is for bias values between 0.1 V (*lower curve*) and 1.0 V (*upper curve*) with bias of 0.1 V. (From 35)

21
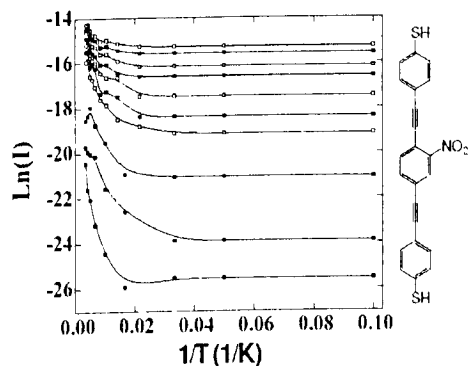
coupling of the system to the thermal environment. The direct tunneling mechanism dominates at low temperatures, where the activated process is exponentially suppressed and activated hopping becomes dominant at temperatures close to ΔE. Selzer et al. [35] have studied the temperature dependence of transport through single olygophenylethynyl (OPE) molecules, with the main results shown in figure 6. At temperatures below 100K the conductance is essentially independent of temperature, as expected for direct tunneling. Above 100K there is a transition to an activated process with linear dependence of the Arrhenius plot. Calculation of the energy barrier for the activated process from the slope of the low source drain voltage curve yields an average activation energy ΔE of 56meV. Both the low activation energy found and the low temperature at which the transition takes place are surprising due to the large HOMO-LUMO gap the molecules are expected to have (larger than 2eV) as the Fermi level is expected to reside near the middle of the gap. Furthermore when applying a bias $V_{sd} \geq \Delta E$ (where one expects to find resonant tunneling) there is still a nonzero barrier to transport in the activation curve. Thus, the energy barrier found is attributed to internal molecular excitations that are not excited by the source drain bias, but become accessible when the temperature increases. The scale of the energy barrier found fits theoretical calculations for the rotation of the phenyl rings of the molecule, which are 40-50meV for the left ring, and 80-100meV for the right.

These measurements serve to shed light on the transport mechanisms affecting transport through molecules. They require, however, careful consideration of the experimental setup: in the presence of inelastic processes there should be some heating of the molecule, making the estimation of the molecular temperature problematic. Temperature changes of the system should also cause thermal expansion and contraction of the electrodes and substrate changing the stress applied to the molecule and the actual distance between the leads; this too could affect the transport.

Methods for single molecule measurements

In recent years several methods have been developed that allow the contacting and measurement of single, or at least very few, molecules. The different methods provide different advantages and disadvantages, both in the characterization of the molecular junction, and in the availability of control of the junction via gating, mechanical tension etc. Gating is a crucial tool to the understanding of the junction energy spectrum, allowing shifting of the molecular levels with respect to Fermi energy at zero source drain bias.

Scanning probe methods

These methods are based on using scanning probe microscopes, specifically scanning tunneling microscopes (STM) or atomic force microscopes (AFM) with a metal-coated tip, to contact single molecules on a conducting surface. While being the most direct approach to the contact and measurement of single molecules these methods are quite limited since it is difficult to determine the electrical contacts to the molecule and gating of the molecule is not readily available.

These methods have proven useful in studying conduction through C60 molecules, due to their large size. Metallic behavior is observed if a good contact is made [36] and by applying pressure to the molecule with the tip it is possible to change its transmission. When the connection to the molecule is made with tunneling junctions on both sides it is possible to make spectroscopic measurements of the vibration modes of the molecule [37].

Scanning probe methods have also been used for the measurement of single molecules embedded in a self assembled monolayer (SAM). In these systems Additional tricks are used to allow the tip to contact only a single
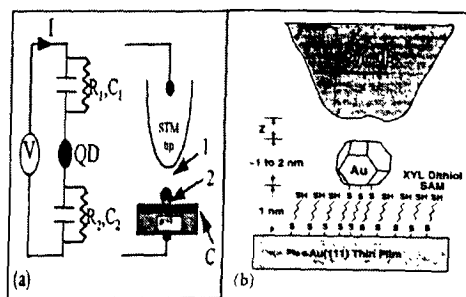

Figure 7: Schematic illustrations of measurement systems using STM to measure molecules. (a) STM measurement of a single C60 molecule from Porath et.al. [37] in a Coulomb blockade setup. (b) Use of a gold nanoparticle to contact only a few molecules in a SAM from Dorogi et.al. [39]

23

molecule, such as embedding only a few molecules with two sides that can bond to gold in the SAM [38], or adding a few gold particles that connect to only a few molecules in the SAM and measuring above them [39].

Improved evaporation techniques

In these methods various tricks are used to get small inter electrode separation that is needed to contact a single molecule. This "direct" approach allows for a relatively straightforward way of creating the gap, and also of gating the molecule. It is; however, very hard to control, or investigate the properties of the contact region or even to make sure that there really is a single molecule there.

Electron beam deposition [40] allows the creation of thin carbon strips with the electron beam that can be used as scaffolding for the electrode evaporation, providing an inter electrode distance of a few nanometers. Shadow mask evaporation [41,42] using thin photoresist
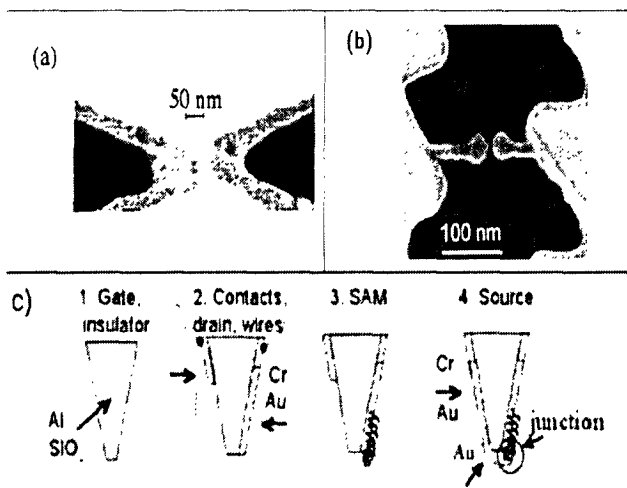
Figure 8: Examples of measurement systems utilizing evaporation techniques to narrow the gap. (a) A field emission scanning electron micrograph of the shadow mask evaporation used by Klein et.al. [41] to decrease an e beam defined gap. (b) An image of the carbon electrodes created using e-beam deposition by Bezryadin et.al. [40]. (c) A schematic representation of the evaporation stages involved in creating the measurement system on a tip by zhitenev et.al.[43]

strips can be used to shrink an e-beam defined structure to few nanometers scale. An innovative technique created by Zhitenev et.al. [43] uses the geometric properties of a square quartz rod. The rod is pulled to create a small tip at the end and the resulting geometry is used to create close contacts and a gate electrode at the tip. In this method gating was observed, but the measurement was not reproduced.

Controlled breaking of the electrodes

In this type of approach one starts with a single thin metallic strip; and breaks it in a controlled way, so as to create a nanometer sized gap.

Mechanically controlled break junctions (MCBJs) were first created by Van Ruitenbeek et.al. [44] and used for molecular measurements by Reed et.al. [45] to measure molecules in SAMs. The MCBJ is formed by creating a thin metal wire on a flexible substrate and bending the substrate until the wire breaks. The two resulting electrodes are covered by a SAM and can then be brought back slowly till electric contact is reached. This method is very reliable, allowing not only contact with the electrodes, but also by gently moving the electrodes it is possible to change the contact between the metal and the electrode thus switching from one current voltage behavior to another [46]. On the other hand gating of the molecule is not readily achieved using this system, nor is the contact area very well defined. Low temperature measurements are problematic due to the fact that the chemical reactions for bonding the molecule to the electrodes occur only near room temperature, and the thermal shrinking of the device during cool down causes loss of contact. Low temperature measurements have been demonstrated [46] by Reichert et.al. by forming the bonds at room temperature, then pulling them apart tearing some gold atoms with the molecule edge, and then cooling down the system and recovering contact.

The electromigration method introduced by Park et.al. [47] relies on the phenomenon where by passing a large current through a thin wire, the wire can be severed in a way that leaves a nanometer sized gap. This method provides a reliable and reproducible way to form molecular scale gaps, it is also possible to measure the system down to cryogenic temperature, and gating is straightforward, allowing for the observation of Kondo physics in transport through spin polarized molecules [23]. However, the shape and crystal properties of the contacts are unclear, and cannot be parameterized well, nor is there any clear way of ascertaining that a single molecule is indeed trapped in the gap.

Lately questions have been raised regarding the validity and reliability of the electromigration method. Recently published works [48,49] demonstrate phenomena highly similar to those observed in molecular junctions, in similarly prepared junctions that contain no molecules. The interpretation provided to these results is that during the breaking process the gold of the wire is broken into small grains, and the

conductance properties observed are actually manifestations of the Coulomb blockade of these grains. This has led to far greater suspicion of the existing methods, and a demand for better characterization.
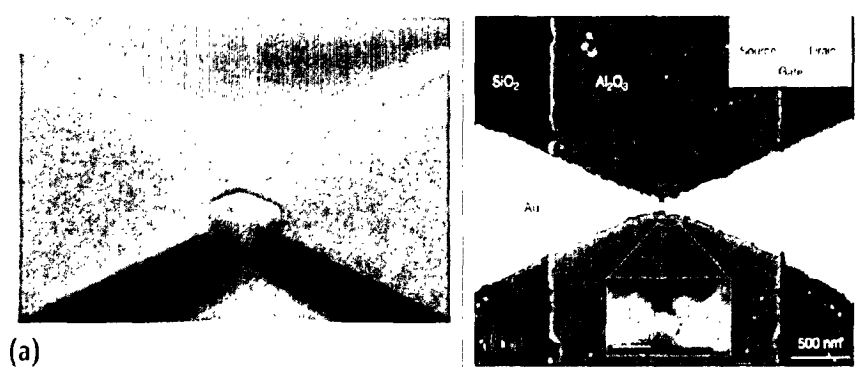

Figure 9: Pictures of electrodes created using controlled breaking techniques. (a) A SEM picture of the MCBJ electrodes just prior to the breaking from Reichert et.al. [21]. (b) A SEM picture (false color) of the electromigration system from Liang et.al.[23], The bottom inset shows a close up of the gap area and the top right a schematic of a trapped molecule between the electrodes.

Conductance histograms

While not, strictly speaking, a distinct method for single molecule measurements; this method represents a very different approach to the problem, and has gained many successes. In this method one makes use of the MCBJ system or the STM to repeatedly form many junctions, so that in some of them there will be a single molecule. One applies a constant low voltage between the electrodes (in the case of an STM between the tip and substrate) then one collapses the two contacts together and disconnects them while monitoring the conductance. This results in conductance plateaus that follow the gradual breaking of the contact. When this process is repeated with molecules present in the vicinity of the electrodes there is a chance that a molecule will be trapped in the gap just prior to breaking, and the molecular conductance will appear as a final plateau. Thus one can gather very large statistics and by creating a histogram of all the data, assign a clear value to the low bias conductance of the molecule. This method has been used successfully to measure the conductance of alkanes and bipyridine molecules at room temperature [50], fully characterize the conductance of the H_2 molecule (As described in the previous chapter) [27] and lately in showing the dependence of conductance in biphenyl

molecules on the angle between the two Benzene rings [51].

In this method there is no ability to fabricate a third gate electrode, but there have been demonstrations of electrochemical gating of molecules in this method [52]. Electrochemical gating is performed in solution; the gate bias is applied between the source and a gate electrode inserted in the electrolyte. The gate voltage falls across the double layers at the electrode-electrolyte interface, leading to an effective gate thickness of a few solvated ions. This enables very effective gating, even reversibly changing the current through the molecule by nearly three orders of magnitude [53]. Unfortunately the requirement that the gating be performed in a liquid makes it possible to make this measurement only at room temperature.
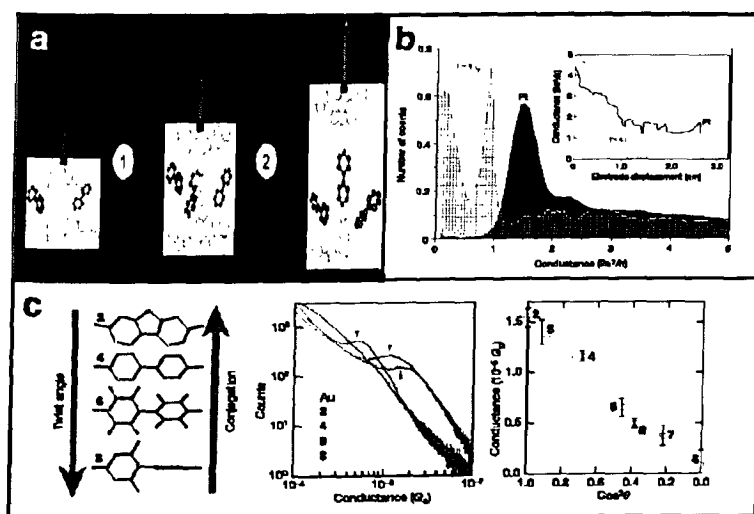
Figure 10: The histogram statistical method. (a) An illustration of the method taken from Li et al. [50]. (b) Histograms of Pt junctions with and without H_2 present in the work of Smit et al. [27]. (c) Change in molecular conductance as a result of twist angle in biphenyls as shown by Venkataraman et al. [51].

The state of the field today

The field of experimental molecular electronics has gained much understanding in the past few years. Researchers have gone from struggling to prove the validity of their methods and struggling to find the right questions to ask, to a position were the relevant questions are becoming clearer and clearer and the ways to address them are also gaining more agreement among the researchers.

Nevertheless there is still far more that is not known about molecular electronics than

what is known. Despite the optimistic claims of Lindsay and Ratner [20], indicating the improvement in correspondence between experiment and theory, there is still disagreement, specifically in the case of small conjugated molecules. The issue of reliable gating of well defined molecular junctions is still very much in question and requires further work. Finally there is still a need for a good method to create stable, well defined molecular junctions with reasonable yield.

The dimer approach to measurement of molecules

While the methods currently in use are quite successful in measuring molecular transport by creating electrodes with molecular scale separation, they provide little control over the number of molecules bridging the gap or the properties of the metal molecule contact. Furthermore most of these systems do not provide a clear way to gate the molecules, and thus are lacking in a very important tool for characterization of the molecular junction.

In developing our method we aimed at a technique that will allow us to trap with high fidelity only a single molecule, while providing better characterization and control over the various elements in our system. We have created a novel method to contact molecules, combining a "top bottom" approach for the creation of electrodes with a separation of a few tens of nanometers with a "bottom up" approach which consists of connecting a single molecule between two metallic nanoparticles (this construct is called a dimer), thus allowing us to bridge the gap between the electrodes. This method provides us with the technological advantage of a straightforward way for creation of many electrodes using conventional parallel processing techniques, combined with the experimental advantage of a well characterized controlled way of connecting a single molecule to well defined gold contacts.
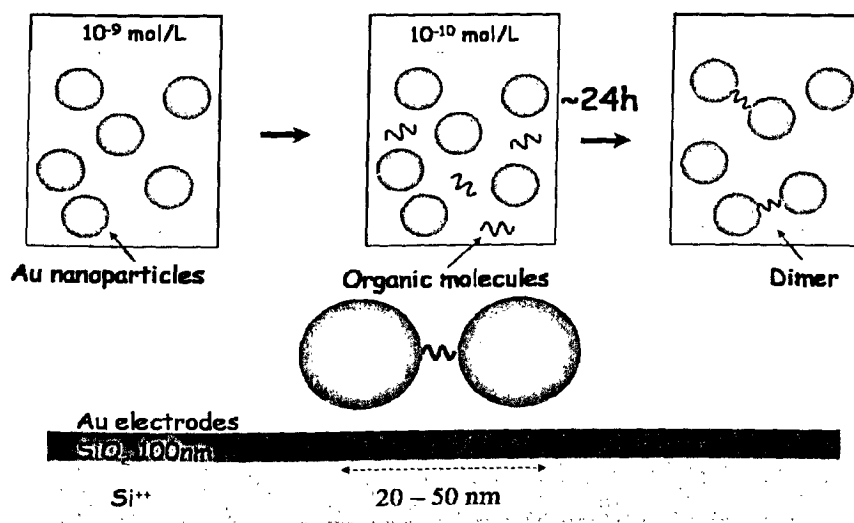

Figure 11 – Schematic illustration of the dimer method. Dimers are formed in solution and then placed for measurement between e-beam defined gold electrodes. A full description of each stage in the process is given in the text.

29

Preparation of the nanoparticles

The gold particles used in our method are created from gold ions in a solution; we use two different procedures for the preparation of the particles:

Large particles with diameters of 30 nm and above are created using a procedure reported by Grabar et al. [54]. The large gold nanoparticles are prepared by enlarging 3nm or 10nm seed nanoparticles using sodium citrate (see the full procedure in appendix A). The size distribution of these particles has a standard deviation of 15-20%, they are polycrystalline and thus don't provide clear crystal facets as contacts to the molecules. Their size, however, is compatible with the readily available e-beam electrodes that have 40 nm spacing, and therefore they were used extensively.

Smaller particles with diameters of 10-18 nm are prepared using a single step process of reduction by sodium citrate and tannic acid [55]. This process creates single crystalline particles with a standard deviation of their size distribution less than 10% and thus provides excellent contacts to the molecules. The narrower size distribution of the particles also allows for better separation of the dimers from higher conjugates in our solution, as will be described in the relevant section.
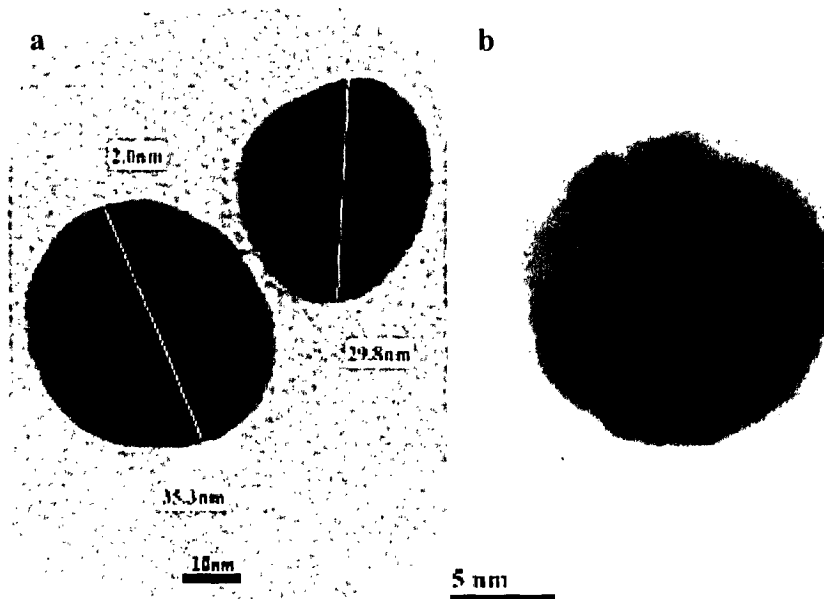

Figure 12:TEM images of gold nanoparticles. (a) A dimer formed from 30nm gold particles (b) A 12nm gold particle. In the case of the smaller nanoparticles the gold crystal structure can be observed, demonstrating that the particles are single crystals.

Preparation of the dimers

Following the synthesis of the gold nanoparticles the solution is mixed with a solution of molecules to create higher order structures. All the spacer molecules used have thiol (SH) groups at two ends, which are known to connect strongly to the gold surfaces forming the hybrid molecule-gold particle objects.

The entire process of dimer formation is done with a very dilute solution (typically on the order of 10^{-9} mol/L) so that the dimers are formed slowly and under well-defined conditions and formation is not affected by small density differences during the initial mixing; at this concentration dimer formation takes several hours. The molecules are first dissolved in a higher concentration solution (typically 10^{-3} to 10^{-4} mol/L) and subsequently diluted to the desired concentration; the process of diluting the solutions is done as fast as possible, taking less than one minute, in order to avoid the molecular polymerization that takes place in the concentrated solution. The solvents used to dissolve the molecules differ for different molecules depending on their polarity (A list of solvents for different molecules is given in appendix B). The molecules are diluted to the desired concentration in a solution of 0.1 mM NaOH. The dilution is done in 3-4 steps of dilution by 2 orders of magnitude at a time, and the solutions are stirred very vigorously after each dilution. The NaOH is a weak base that serves to promote the removal of the hydrogen atoms from the thiol end groups of the molecules, allowing them to bond with the gold surface of the nanoparticles. As will be explained in the next section we want to use a ratio of 10 particles per molecule, we have found that it is best done by using equal concentration solutions and different amounts. We add 500µL of molecule solution to 5 mL of gold particle solution, and immediately upon adding the solution we stir the combine solution vigorously to achieve a homogeneous molecule and gold particle solution. We let the solution stand under refrigeration for a full 24 hours, to ensure that all the molecules form dimers. When the two solutions are mixed together the molecules connect to the particles, as illustrated in figure 13b, forming complex structures where two or more particles are connected together (figure 13c-e). The appearance of higher level conjugates in the solution together with our use of a dilute solution of molecules serves to reassure us that there is only one molecule bridging each two particles. The low density of molecules in the solution relative to that of the particles creates a situation where once a molecule attaches to a particle it will with high probability connect to another

particle forming a dimer, before another molecule can situate itself on the same facet. If another molecule attaches to this dimer, it is likely to connect to a different facet of the particles and attach itself to another particle, thus forming a higher-level compound object. Transmission electron microscope (TEM) imaging allows us also to view the gap between two particles and to verify that the distance between the particles is indeed of the order of the length of the molecule used. Fig 13a shows such an image of a dimer with a benzene dimethylethiol (BDMT) molecule bridging the particles, as can be seen the distance between the particles is about 1 nm, which is the length of the molecule. Another important feature of figure 13a is the visibility of the crystal lattice of the gold particles forming the dimer.
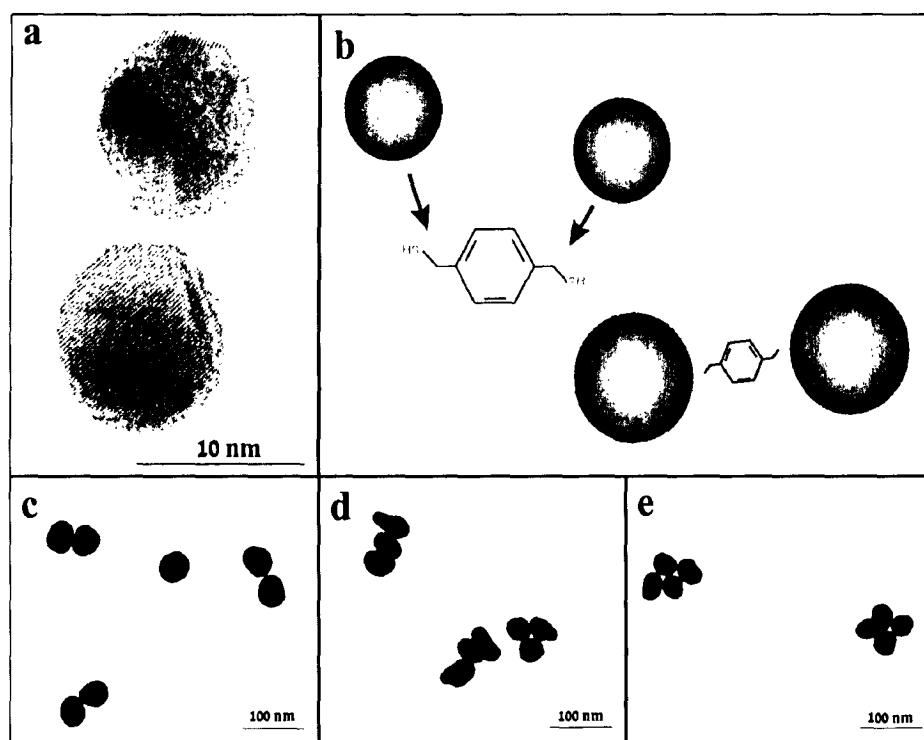

Figure 13 – Dimer formation. (a) A high resolution TEM picture of a dimer BDMT dimer, showing the 1nm gap. (b) Illustration of dimer formation in the solution. (c-e) TEM pictures of dimers, trimers and tetramers.

To ensure that most of the dimers are bridged by a single dithiolated molecule, the concentration of the latter (Cm) in the reaction mixture should be much smaller than

the concentration of the single gold particles (Cp). In that case, when the reaction is completed, the ratio R of dimers to the total number of particles in the solution (including those bound to molecules) should equal the ratio of molecules to particles $R \approx Cm/Cp$. We measured R for different input concentrations of dithiolated molecules, keeping Cp fixed, and found that the above relation holds for Cm:Cp ratios that are lower than 1:10 as shown in figure 14. We take that as an indication that below this ratio there is indeed only one molecule in each dimer, as required. In order to obtain the best yield we would like to maximize the percentage of dimers in our solution, so as to get a higher amount of trappings, thus we have chosen to use a 1:10 ratio in the dimer creation process. This estimate ignores the creation of higher conjugates in the solution, but up to a ratio of 1:3 molecules to particles there were no more than 5% trimers and 1% tetramers, so that they are not significant in the analysis.
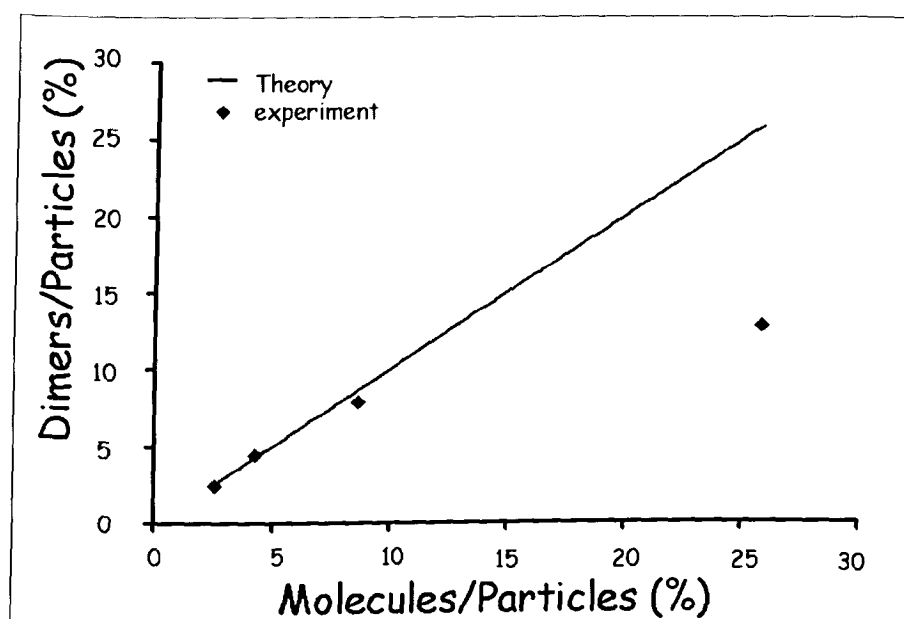

Figure 14- Effect of molecule-nanoparticle ratio. The percentage of dimers in the solution as function of the percentage of added molecules. Up to a 1:10 ratio there is a good fit with the prediction for a case of a single molecule per dimer.

Surface enhanced Raman spectroscopy of the dimers

Inelastic light (Raman) scattering gives information on the vibration degrees of freedom of a molecule. Unfortunately, the typical cross sections per molecule are extremely weak, of the order 10^{-30} cm^{-2}, yielding a practically undetectable signal. A way out of this was suggested by using the enhancement of Raman scattering near metal surfaces. It is well known that a dramatic signal increase may occur if the molecule is adsorbed to metal particles of sub-wavelength dimensions. This technique, known as surface enhanced Raman scattering (SERS) [56], has been demonstrated to enhance the effective Raman cross section by a staggering 14–15 orders of magnitude. This huge enhancement has proven enough for successful single molecule spectroscopy. SERS can be used as an independent tool for studying the properties of the molecules in the dimer; it can also serve as decisive evidence that the dimer is indeed bridged by the molecules.

Raman spectroscopy measurements on dimers are done by Tali Dadosh, a PhD student in our group, in the laboratory of Professor Gilad Haran in the Weizmann institute chemical physics department. The dimers for the measurement are formed using a polythiophene T4 molecule (see inset to figure 15a) with silver nanoparticles. We use silver particles instead of gold because these have been shown to give a stronger enhancement to the Raman signal [57]. For a full description of the synthesis and measurement methods see reference 58.

Figure 15a shows the SERS measurement performed on a silver dimer. Comparing the SERS data with regular Raman spectroscopy performed on the T4 molecules in a powder (inset to figure 15a) we see that most of the peaks that appear in the powder spectrum also appear in the SERS spectrum. The only exception is the peak at around 2100 cm^{-1}. The powder contains T4 with a thio-ester protecting group; this group is cleaved before the reaction with the Ag nanoparticles is performed. The peak around 2100 cm^{-1} probably belongs to this leaving group or more specifically to the sulfur.

After taking the measurement of the Raman signal, samples are taken for examination in the SEM. We correlate the finding of a clear T4 spectrum with the presence of a dimer at the spot; we have found that the existence of a Raman signal can always be correlated to the presence of a dimer or higher conjugate.

Figure 15- SERS measurements on dimers.

(a) SERS signal from a silver dimer. Insets show the chemical structure of the T4 molecule, and a Raman spectrum taken from the molecules in a powder. (b) Optical microscope image of a square of the marked sample which contains a single Raman signal (the bright spot). (c) SEM image of the same square. In the same location of the Raman signal spot a clear dimer is observed (insert), all other objects in these square are single nanoparticles.
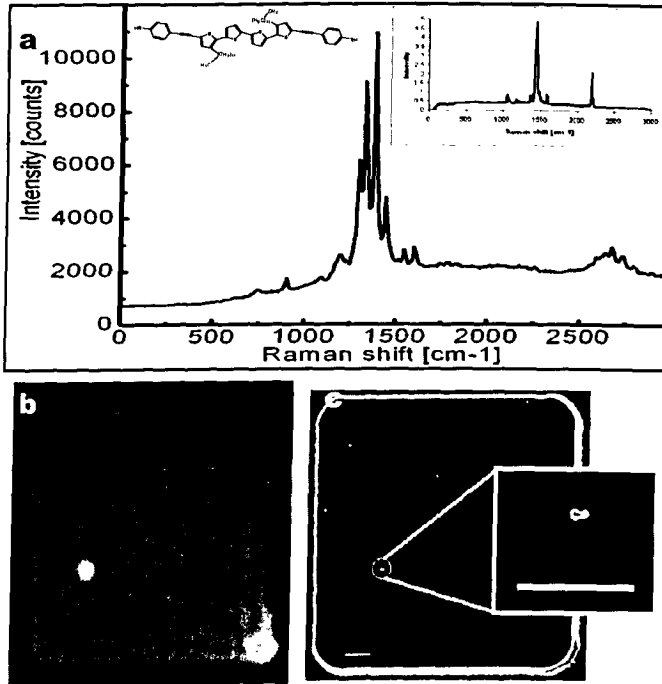
Acetyl protected molecules

A common problem with thiolated molecules is their tendency to form polymers through sulfur-sulfur bonds; this leads to degradation of the molecules and can create great uncertainty in the measurements. This problem is usually solved by using molecules, which are chemically protected by acetyl groups that are connected to the thiols. The acetyl groups shown in figure 16 are attached to the sulfur atoms on both edges of the molecule. The acetyls cap the thiol groups and prevent molecular polymerization in the powder; just prior to the attachment of the molecules to the gold surfaces they are removed by the addition of a base. This way as the sulfur atoms are revealed by the base they immediately connect

Figure 16 – Chemical structure of an acetyl group $COCH_3$ The R represents the place where the molecule is attached.

to the gold surface. This method works well in creation of SAMs were there is no problem with the deprotection of the molecules in the presence of the gold surface, however in our system we have found that it is problematic, the bases used for the removal of the acetyl groups tend to attack the gold nanoparticles causing them to aggregate. On the other hand, one could try to deprotect the molecules separately
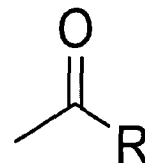
prior to dimer formation, and dilute the solution before adding it to the gold particles. We have tested the state of the molecules in solution after deprotection using mass spectrometry and have found that five minutes after the deprotecting agent is added there is already a formation of a large number of molecular dimers; this is long before there is full deprotection of all the molecules. This means that in solution, without presence of a gold surface to connect to, the molecules polymerize faster than they go through the deprotection process, invalidating this approach. This has led us to conclude that the use of acetyl-protected molecules is impossible in our system. We prepare the molecule with the acetyl protection, so that they will be preserved for a reasonably long time, and deprotect small amounts using the method reported by Tang and Schneider [59]. Deprotected molecules are kept in a freezer under inert atmosphere, so as to minimize their polymerization, and replaced every two months. The molecules are checked regularly using mass spectrometry to ensure that they have not undergone significant polymerization, and are replaced when there is significant degradation in their quality.

Concentration of the dimers

After the 24 hours of dimer formation are past the resulting solution is separated in a gradient to increase the percentage of dimers. The solution is placed at the top of a tube containing a glycerol gradient and centrifuged so that the different conjugates travel down the tube at a rate dependant on their mass (for more details see appendix C). This leads to the creation of bands in the tube containing different percentages of dimers in them, the bands can be seen in a demonstration of this method using two different sizes of particles (figure 17a). The solution is extracted from these bands using a gradient separation technique, which allows us to separate the fractions without mixing the solution, and studied using a TEM or a SEM, to verify which type of conjugates occupies each band. We have found that while the TEM provides better imaging of the particles the preparation method for the TEM samples can leave small droplets of solutions that can dry and form "fake" aggregates. Samples observed in the SEM are prepared by placing a drop on a GaAS chip for 1-2 minutes, washing it of with distilled water and blow drying with nitrogen, thus preventing any formation of spontaneous dimers. GaAs is used due to its availability and the good contrast of the gold particles on it. Typically we are able to obtain solutions containing 40-60%

dimers depending on the particle size and their size distribution; these fractions also contain 5-10% trimers and higher conjugates. We select for trapping and measurement the fraction that has the largest concentration of dimers, with the least amount of higher conjugates. The presence of single particles in the solution is not very problematic in our system, since they are easily identified in their transport behavior, and usually are not large enough to bridge the gap. Figure 17b shows an example of the percentages of dimers and trimers in the different fractions; clearly in this case fraction 3 would be chosen for measurement.
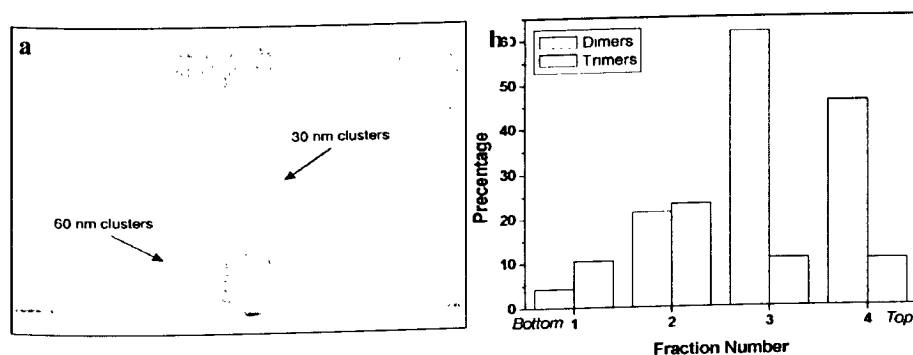

Figure 17 – The gradient separation method. (a) Gold nanoparticles of different sizes separated by centrifugation in a glycerol gradient. Right: the upper band is of 30 nm gold particles, the lower band is 60 nm gold particles. Left: only 60 nm gold particles. (b) The percentages of dimers and trimers in different fractions in a gradient.

The solutions that are extracted from the gradient contain a large percentage of glycerol, leading to a high viscosity of the solution; this damages our ability to attract the dimers to the area of the gap between the electrodes. In order to clean the solution we dilute it with double distilled water at a 9:1 ratio and concentrate the dimers at the bottom of the tube using centrifugation, the parameters of the centrifuge are chosen so that the majority of the dimers will be collected, but there will not be any spontaneous aggregation of particles in the solution due to the high density created. This is tested by comparing the percentage of dimers in the solution before and after centrifugation. After the centrifugation the supernatant is removed and discarded. This process of cleaning the solution is repeated at least three times before the solution can be used. After the cleaning process we are left with 10-20μL of solution for trapping, which is kept in a refrigerator at 4° centigrade until use.

Fabrication of the electrodes

E-beam defined electrodes

The direct way of making the electrodes is based on the use of conventional e-beam lithography for the definition of the electrodes. This allows for good control of the electrode shape, enabling us to plan them so that they can focus the field gradient and best attract the dimers to the electrode gap, the planar configuration of the electrodes also allows straightforward imaging of the samples in an SEM. We plan the layout of the electrodes so that the active area where the electrode edges are located is small (see figure 18) so that we can use a very small drop of solution for the trapping.

The e-beam writing is done on a 2.5 by 2.5mm wafer of highly doped silicon with a 100nm silicon oxide layer grown on top of it. This allows us to fabricate 64 dies of 12 electrodes in a single writing. The oxide layer is of a very good quality, allowing the application of a gate voltage above 40V without any noticeable leakage. The substrate can thus be used as a back gate to control the conductance through the system in a standard single electron transistor configuration. The main drawback of this method is that in using it we are limited in the obtainable electrode spacing by the resolution of the e-beam lithography. We are capable of creating reproducible electrodes with a spacing of 25nm or more.

The electrodes are defined using standard e-beam technology (see appendix D for the full procedure) after development of the resist we evaporate the electrodes using gold with a nickel adhesion layer. We have chosen to use nickel as the adhesion layer due to our need to use an ozone stripper to clean our samples; we have found that other metals like titanium and chromium, commonly used as adhesion promoters, are damaged by the ozonation, causing peeling of the electrodes at the edges. After evaporation the chips are coated by photoresist to protect the electrodes and diced; the photoresist is left until the die is used, and then removed with acetone.

The contact to the gate is formed by etching the oxide in buffered hydrofluoric acid for 2 minutes to expose the silicon, evaporating a micron thick layer of aluminum on it and annealing it at 460°. This forms contacts to the silicon that remain conductive at 4 degrees Kelvin; at a 1V bias we usually get a resistance of 10-100KΩ through 2 mm of silicon. After annealing we evaporate a layer of gold on top of the aluminum to improve our ability to bond to the pads. An alternative way of contacting the substrate is by scratching the oxide with a diamond scriber and pressing a small indium dot to

the scratched area. The indium can be smeared over the surface and connected to a gold pad, which can then be bonded. This method is somewhat cruder than the previous one, but it provides contacts with approximately the same conductivity.
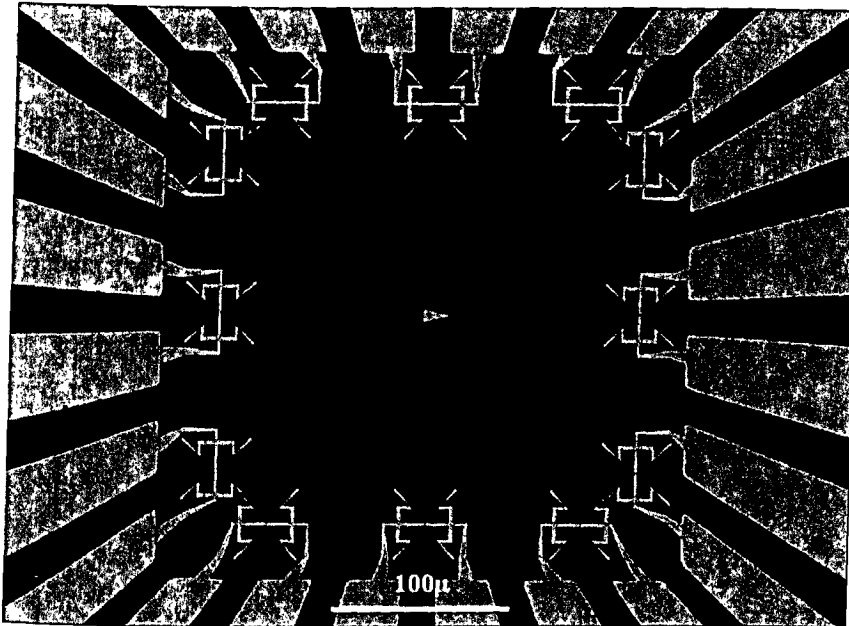

Figure 18 – SEM image of a die of 12 electrode pairs, the area used for the electrodes is approximately 300um by 300um, allowing use of a minimal amount of the solution

MBE defined electrodes using selective etching

Another method we have used to create closely spaced electrodes is by using selective etching of a GaAs-AlGaAs heterostructures created in a molecular beam epitaxy (MBE) system [60]. These crystals serve as scaffolding for the creation of the electrodes. The use of MBE defined crystals allows us to go beyond the limits of e-beam lithography and to achieve electrode separation in the range of 5-50 nm. The process is shown schematically in figure 19.

The wafer used consists of two thick layers of $Al_{0.3}Ga_{0.7}As$ with a thin layer (5-50nm) of doped GaAs sandwiched between them. The wafers are first etched to form mesas and expose the wall. In our early samples [60] the etching was performed in phosphoric acid. The mesa edges formed using this method are slanted due to the isotropic etching; this causes the top part of the gap to be very weak and unstable. We have found that the results are significantly improved when the etching is done anisotropically using ion plasma etching; this results in nearly vertical walls yielding

symmetric electrodes on both sides of the gap (figure 19a). After the cross section of wall is exposed the wafers are etched in citric acid and hydrogen peroxide (4:1) that selectively etches the GaAs (the bulk selectivity is 1:90 [61]) to form a small gap with a width approximately like that of the original GaAs layer (figure 19b). The etching is done for a period of 2 minutes to achieve an etching depth of 50nm; this is necessary to prevent the electrodes on the mesa edge from contacting the conducting GaAs layer, this is particularly problematic in the back of the mesa where the evaporated metal is thicker (Figure 19d). When attempting to create smaller gaps (5-15nm) we have found that the gap does not penetrate horizontally more than 15-20nm; we have attributed that to an inability of the etchant to penetrate the gap properly. However we have found that by performing the etching with the tube dipped in a sonicator bath we have been able to reproduce the etching depth of the wider gaps.

Ohmic contacts are evaporated on top of the mesa, and alloyed to form electric contacts with the doped GaAs layer, which then serves as a third electrode that can provide gating of the molecules bridging the gap. Finally PdAu is evaporated on the wafer at three different angles to form continuous electrodes at both sides of the gap (figure 19c-d). This is done using a rotating stage, which allows rotation of the sample without breaking the vacuum. The initial alignment of the sample for evaporation is done using a laser pointer mounted on the stage to properly align the sample in the direction of the PdAu crucible in the evaporator. The first evaporation, of a 7nm layer of PdAu to minimize the chances of shorting to the gate, is done at a right angle with the mesa edge to coat the gate layer and remove the depletion region at its edge; this has proven crucial in allowing efficient gating of trapped structures. Two more evaporations are done to form a continuous connection over the back part of the mesa; these are at a thickness of 50% more than the gap size to ensure covering of the gap.

This method provides excellent control of the gap size, and allows fabrication of closely spaced electrodes, up to 5nm apart. We have found however that for the goals of our experiment it is problematic. The lack of ability to control the shape of the electrodes near the gap makes the trapping process less reliable, the fact that the electrodes are not planar causes dimers to be attracted also to places where there is a curvature of the electrodes, such as when they climb up the mesa, and finally the electrodes are less stable causing a large amount of cases where the electrodes peel near the gap upon trapping. Since we do not need to have electrodes that are so close together we have chosen not to use these electrodes much in our system. Modified

versions of this method are however used by other groups to measure proteins [62] and colloidal nanoparticles [63].
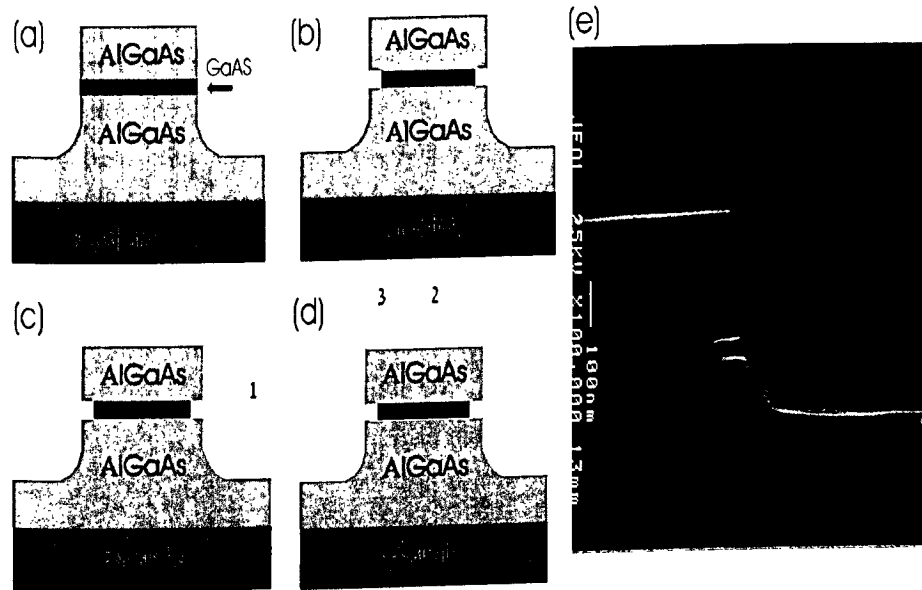

Figure 19 - Preparation of the electrodes. (a) Plasma etching creates mesas with steep walls, exposing the profile of the MBE growth. (b) Selective etching in citric acid forms few nanometer scale gaps. (c) The first evaporation of PdAu creates two electrodes with a small gap, while also adding a coating of PdAu on the doped GaAs region, improving its gating capabilities. (d) Two more evaporations form continuous electrodes bridging the gap on the other side. (e) A SEM image of a 50 nm gap formed using this method.

Positioning the dimers between the electrodes

In order to place the dimers for measurement between the electrodes we use the method of dielectrophoretic trapping introduced by Pohl [64]. In this method a voltage is applied between the electrodes inducing a dipole moment on the dimers. The dimers are then attracted by the dipole-dipole interaction to the area between the electrodes, where the field gradient is largest. If the particle being manipulated is much smaller than the characteristic distance of the variation of the applied electric field the average force felt by a particle with a dipole moment m in a field E is given by $\langle F \rangle = 0.5 \Re\{m \cdot \nabla E^*\}$ with the $\Re$ signifying the real part of the expression in brackets. For a spherical particle with radius r and permittivity ε_p in a medium with

permittivity ε_m the induced dipole moment is of the value $m = 4\pi|\varepsilon_m|r^3\left(\dfrac{\varepsilon_p^* - \varepsilon_m^*}{\varepsilon_p^* + 2\varepsilon_m^*}\right)E$.

Thus the resulting force applied to the particles in the solution is

$F = 2\pi|\varepsilon_m|r^3\Re\left(\dfrac{\varepsilon_p^* - \varepsilon_m^*}{\varepsilon_p^* + 2\varepsilon_m^*}\right)\nabla E^2$, the term in the brackets is the Claussius-Mossoti

factor whose value can dictate whether the applied force will be attractive or repulsive depending on the frequency. In our case the dimers have a polarizability, which is clearly higher than that of the surrounding medium leading to an always positive trapping force. A significant limitation to the effectiveness of the trapping process is the influence of the Brownian forces in the solution. The force applied by the dielectrophoretic trapping diminishes as the particle size cubed, causing a situation where below some size the random Brownian motion will dominate and trapping will not be effective, however due to the closeness of the electrodes in our system the electric field gradient is large enough to overcome this Brownian motion.

Dielectrophoretic trapping of metallic nanoparticles was first reported by Bezryadin et.al. [65], using a DC applied voltage for the trapping. In our case the gold particles are negatively charged, due to remaining counter-ions on their surface, and a DC voltage attracts them to the positively biased electrode (figure 20a). Applying an AC voltage instead, allows us to avoid this problem.

A further complication arises from the existence of electric field induced motion of the fluid near the electrodes; this has been attributed to the effect of the field on the double layer formed by the ions in the solution reacting to the applied voltage of the electrode [66]. While it has been suggested that this effect can be used for particle separation, in our case it causes the particles to be swept away from the gap. The fluid flow near the electrodes has been shown by Ramos et al. [66] to be frequency dependent usually reaching a maximal value in the KHz range, and decaying after that, the effect of this motion can be seen in figure 20b-d.

Finally the AC field also has the effect of electrorotation, causing the dimers to align their long axis, with the larger dipole moment, with the electrodes. We have found that this effect is more pronounced the higher the frequency of the applied trapping voltage, up to a frequency of 10MHz.

Due to the two last effects we have chosen to use a frequency of 10MHz, were we have been able to obtain effective trapping with as little as 800mV applied to the

electrodes, and good alignment of the dimer with respect to the gap as can be seen in figure 20c.

The requirement of trapping only a single dimer is quite demanding; the parameters needed for trapping differ slightly from one dimer solution to the other, depending on their concentration. Therefore we test each solution first to ascertain which parameters give the best yield of single trapped dimers by observing the samples in the SEM for the highest yield; we then use the same parameters for that solution until it is finished.

Figure 20: SEM images of trapped particles under different AC frequencies. The trappings in a-d were performed with a voltage of 2V for 1 min. (a) Trapping with a DC voltage, all the particles are attracted to one electrode due to their charge (b) Trapping at a frequency of 1 KHz (c) Trapping at 10 KHz (d) Trapping at 50 KHz. (e) trapping of dimers at 10MHz with 1Vpp for 30 sec.

A crucial stage in the dimer trapping procedure is the cleaning of the electrode surface between the electrodes and the gold particle but it also affects the yield of the trapping. The samples are first placed in hot trichloroethane (TCA) and in hot acetone for five minutes each, and then rinsed in methanol. The samples are placed in an ozone stripper for 7 minutes at 70°; this is done in order to remove remains of polymerized photoresist left over from the lithography. The photoresist in the area near the edge of the metal electrodes is subject to some exposure during the lithography and usually some of it is left; since this is the active part of our sample it is crucial to remove any traces of resist from it. Finally the samples are rinsed in

ethanol while stirring gently for 8 minutes. This final step is necessary to remove the unstable gold oxide layer, which is formed during the ozonation process [68]. Failure to remove this layer results in samples where even if there is a dimer bridging the gap there is no conduction through the system.

After cleaning the samples are taken to a home built probe station, where the trapping takes place. The probe station used is made of Karl Suss PH150 probes mounted on a platform, which are connected to an Agilent 3120A arbitrary signal generator via very short coaxial cables to minimize parasitic capacitance. The probe station is used exclusively for trapping since we have found that any changes made to it can change the parasitic capacitance and hence the trapping parameters. The trapping is performed using a high frequency sinusoidal signal and therefore is very strongly influenced by parasitic capacitances in the system. A $0.35\mu L$ drop of solution containing dimers is placed on the sample and the trapping signal is applied for a period of 30-90 seconds to each electrode pair in turn. We try to perform this with the maximal speed, to avoid drying of the drop that can decrease the reproducibility of the trapping. When the drop starts to decrease we immediately add more of the solution to prevent significant changes in the density of the solution during trapping.

After the trapping is performed the sample is washed with distilled water, blow dried with nitrogen and measured at room temperature up to 1.5-2V on a probe station, electrode pairs that exhibit non zero conductance are considered "suspect" of having trapped dimers. The sample is glued to a 24-pin header with photoresist; the suspect electrodes are bonded and measured in a liquid helium container.

Bonding is done without any heating of the substrate to avoid damage to the trapped molecules. Great care needs to be taken to ground anything that comes in contact with the samples after trapping is complete; the samples are extremely sensitive to electrostatic discharges, which cause the electrode edges to peel near the gap.

Differentiating between samples that contain dimers and those that are bridged by single gold particles is easy to do from their low temperature behavior. To remove samples containing many dimers and ascertain that we do not misunderstand our low temperature measurements we observe the samples in the SEM after measurement; devices containing many dimers are not included in our final analysis.

An interesting observation from the SEM measurements is the correspondence found between the dimer brightness in the SEM image and the conductance of the dimer. We have found that dimers that are similarly situated at the gap can give very different conductance values, high conductance values are in the 10^{-8} Siemens range whereas the low conductance ones are in the range of 10^{-10}-10^{-11} Siemens. All the high conductance dimers appear as bright images in the SEM while low conductance ones are a duller color. We interpret this as an indication that the brightness of the SEM image is a result of good contact between the gold particles and the electrode [67], meaning that the low conductance of the duller dimers is a result of a bad connection to the leads. We therefore do not include these samples in the data that we use.
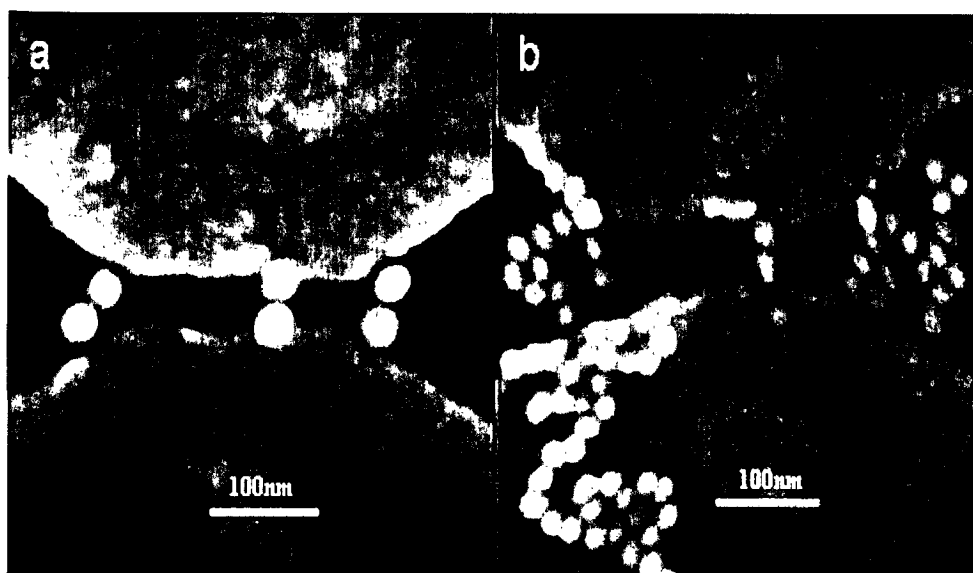

Figure 21: SEM images of bright and dark dimers. a) A bright dimer, that gave a current of 7nA at 1V source drain bias. b) A dimer and several other trapped aggregates, all dark, this sample gave 100pA at 1V.

Electrical measurement setup

Measurements at 4K are performed by dipping the sample directly in a dewar of liquid helium. This method is fastest, and allows a large turnaround of samples necessary for focusing on those that exhibit molecular features. The samples are placed on a measurement rod that allows them to be inserted into a helium dewar.

Measurements at temperatures higher than 4K are performed using a 1.5K cryostat, shown in appendix E. The cryostat is essentially a tube separated from the helium in

the dewar by a vacuum sleeve. Helium is admitted to the inner chamber through a needle valve at the bottom of the cryostat, where the sample is placed with a rod. The cryostat is capable of reaching temperatures below 4K by pumping on the helium in the inner chamber, but we have found that this does not significantly change the properties of the molecular junction. Generally one controls the temperature of the sample by running a current through a heating coil at the end of the rod. We have found that this heating causes a large increase in the noise level of the sample; therefore we perform temperature dependent measurements simply by closing the needle valve and allowing the chamber to warm up gradually while monitoring the temperature using a lakeshore 3310 temperature controller. Some experience is needed to perform these measurements well and avoid drastic changes in the warming up rate; typically one starts by closing the needle valve only partially since the early stages of heating are quite rapid, the valve needs to be closed further at ~20K and again at ~70K (these points may vary from system to system). The 1K cryostat allows controlled warming of the samples up to temperatures of ~250K (depending on the quality of the vacuum in the insulating sleeve), but we have found that our samples become too noisy to observe features past ~120K.

Measurements of conductance and current versus voltage plots are performed simultaneously using a standard lock-in technique: a small AC signal from an EG&G 7260 DSP lock-in is added to the source drain voltage from a Yokogawa 7651 DC source connected to the source electrode. The drain electrode is connected to a Keithley 428 current amplifier and from there to a HP 34401A multimeter to measure the DC current and back to the lock-in amplifier to measure the in phase response of the molecule to the AC excitation. In this manner one measures the current and its derivative simultaneously. The frequency of the excitation is chosen to avoid the frequencies, at which the system has much noise, checked with a spectrum analyzer we measure at 67 Hz, avoiding the 50 Hz frequency of the electric lines and a 15 Hz disturbance found in our system.

We have found that the rate at which we scan the source drain voltage as well as the magnitude of the excitation are very significant factors in the amount of noise in the measurement, we therefore aim to ramp the applied DC voltage as slow as reasonably possible, and to keep the excitation at the minimum value that can allow us to observe a good signal.


Effect of the scanning electron microscope on the samples

Observation of the dimers in an SEM often causes drastic changes in their conduction properties. We have found that samples observed in the SEM had become highly

conductive and lose all of the features that we attribute to the molecules. This is probably because the electron beam of the SEM damages the molecule either directly by bombardment of the molecule itself, or by causing discharge across the molecular junction between the two nanoparticles. We have found that if the scan is performed quickly enough and at a low acceleration voltage it is possible to reduce the damage to the samples and still observe the molecular features after scanning. An interesting observation is the fact that while the molecular features remain roughly unchanged after this process, the overall conductance of the junction is increased by as much as two orders of magnitude; this can be seen in figure 22.

It does not seem reasonable to assume that the observation of the sample by the SEM can improve the connection of the molecule to the gold nanoparticles, furthermore it is extremely unlikely that this could happen without completely altering the molecular features. The SEM may however cause damage to the ligands coating the particles, either directly or by charging the particles, forcing them to discharge though the ligands. Therefore we assume that originally most of the voltage drops across the electrode-gold particle interface and scanning in the SEM improves that contact causing the molecule to become the bottleneck to conduction. Thus we believe that the SEM can be used to change the electrode particle contact, providing another knob allowing more control of the system.

Figure 22 SEM influence on samples. Measurements of a molecule before (black curve, corresponding to right axis) and after (red curve, left axis) scanning in a SEM. The general molecular features and the width of the peaks remain unchanged, while the overall conductance is increased by nearly two orders of magnitude.
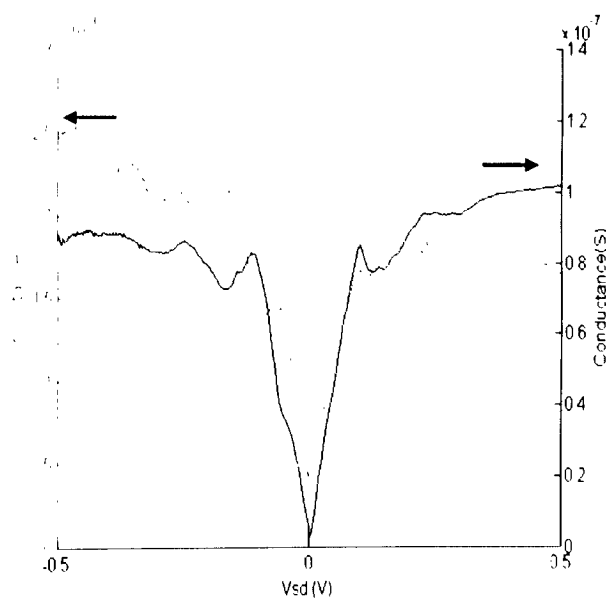
Measurements on single nanoparticles

In order to understand and characterize the system we started by studying the transport through single particles, where the physics is well understood. In the solution the particles are covered by a thin coating of ligands, which serve as stabilizing agents to prevent aggregation, these serve also as tunneling barriers between the particle and the electrodes, thus forming a configuration of a small metallic island weakly coupled by tunneling between two electrodes. In such a system we expect to observe CB phenomena as described in the introduction. The charging energy of the particles depends on their self capacitance, which is proportional to their diameter and on their capacitance to the electrodes, which should also scale with their size.

The study of transport through single nanoparticles was performed on mesa structures and not on the e-beam defined structures that we use for the dimers. The different geometry of these electrodes causes the capacitances of the particles to the leads to be different leading to different charging energies of the particles and the conductance values shown will also be quite different in the e-beam defined electrodes. However the general phenomena of scaling of the energy with particle size should be the same for any system studied. Current voltage features of a 10 nm gold particle are presented in figure 23a. A clear gap is seen at source drain voltage –25mV<Vsd<25mV, a Coulomb staircase is seen at higher voltages with a period of approximately 50 mV. The periodicity found fits with a capacitance of approximately 3aF, this is about one order of magnitude larger than the self-capacitance of a sphere of this size $C=4\Pi\varepsilon_0 R\approx0.5aF$. The difference is due to the fact that the capacitance defining the steps is the total capacitance including the capacitance to the
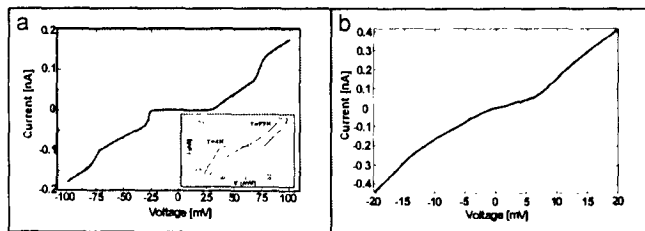

Figure 23 – Coulomb blockade of single gold nanoparticles. a) IV of a 10 nm diameter gold particle, showing a 50 mV gap. The insert shows the temperature dependence between 4K and 77K. b) IV of a 60 nm gold particle, showing a gap of ~10mV. All measurements were performed on mesa etched electrodes.

electrodes. The inset shows a different sample measured at two different

48

temperatures, at 4.2 K a clear gap is seen, the size of the gap is bigger than that of the previous particle, due to random differences in the capacitance to the nearby electrodes. At 77 K the thermal energy available to a tunneling electron is large enough to smear out the gapped region completely, but there is still a distinct non-linearity in the curve as a remnant of the gap.

For comparison we show in figure 23b a measurement that was performed on a 60 nm gold particle. Here the gap is smaller (~10mV), as is expected for a larger particle and the conductance inside the gapped region is not zero. This nonzero conductance is a result of the fact that the smaller gap makes the temperature at which the smearing occurs lower, and the 4.2K at which we measure is not enough to completely freeze out transport in the gapped region. As can be seen the charging energy of the particles does indeed scale roughly with the particle size.

Molecular conductance

Establishing that current goes through the dimer

When performing nanoscale measurements it is very important to ascertain that the transport is indeed taking place in the path that one anticipates. The small distances over which transport takes place can allow current to go through dirt on the surface of the sample. An advantage of the dimer method is our ability to correlate the presence of dimers or nanoparticles in the gap and the existence of a finite conductance. After measuring hundreds of samples we have seen that in all the cases where we found a significant conductance (Above 10^{-13} Siemens) there was a dimer or a nanoparticle in the gap.

Our measurements of conjugated molecules show (as will be discussed) high energy peaks. In several of our measurements we are also able to observe oscillations on an energy scale fitting that expected from the nanoparticle CB (figure 24). The periodicity of these peaks is ~50mV, fitting to a capacitance of 3aF, since the self capacitance of the 30 nm particles is 1.5aF this can be explained as the

Figure 24 – Signature of the nanoparticle charging

High frequency CB oscillations superimposed over the molecular spectrum.

charging energy of the single nanoparticles modified by the capacitance to the electrodes. Thus it is clear that the transport through our system does indeed go through the dimer.

In the following section on the gating of molecules we will show that by observing the response of these high frequency oscillations to an external gate voltage we can demonstrate that the transport takes place through two dots in series, exactly as we would like.

Effect of conjugation on molecular conductance

When studying transport through single molecules we expect to see beyond the regular Coulomb blockade effects of the clusters also the properties of the specific molecule. As said in the introduction part we expect current through a molecular system to be enhanced when the molecule has available electronic states at the Fermi energy of the leads. For the achievement of elastic transport it is also necessary for
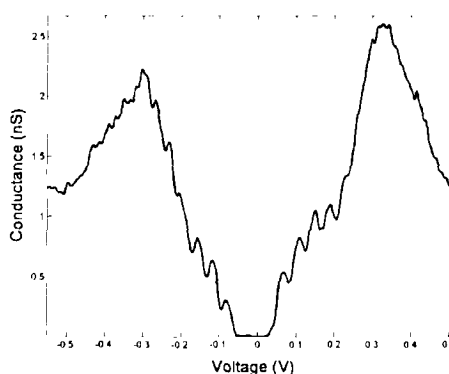
these states to be extended in order to allow the electrons to travel freely through the molecule. This requirement is satisfied nicely in the case of conjugated molecules; these have delocalized electron states along the molecular backbone and are also usually rather stiff, making them ideal candidates for measurement in our system

The importance of extended electronic states for molecular conduction is well established; we decided to focus on the effect of localization centers added in a conjugated molecule. We studied the electrical conduction through three short organic molecules (shown in the inset of figure 25): A fully conjugated molecule, 4,4'-biphenyldithiol (BPD) where the only reduction in conjugation arises from the angle between the two phenyl rings, Bis-(4-mercaptophenyl)-ether (BPE) in which the conjugation is broken at the center by an oxygen atom, and 1,4-benzenedimethanethiol (BDMT) where the conjugation is broken near the contacts by a methylene group. The BPE molecules is an example of a case where the conjugation of the states in the molecule is broken, whereas the BDMT still has a fully conjugated central part but the overlap of its electrons with the leads is reduced due to the methylene. We have been able to measure a total of: 15 BPD, 13 BPE and 15 BDMT devices

Figure 25shows a comparison of the differential conductance of the three molecules at 4K. These are representative curves from more than ten devices of each of the molecular species that were studied. Looking first on the difference in conductance among the molecules we can see that this is quite pronounced: The BPD molecule shows a more or less linear rise in conductance (superimposed with peaks that will be discussed later), the conductance at 0.5V is already at approximately 1nS. The BPE and BDMT dimers show remarkably different behaviors. It is clearly seen that the conduction through the dimers formed from these molecules turn on at much higher voltages (typically larger than 0.5V) and one cannot resolve any peak structure.

The systematic difference between the three molecules further confirms that the measured differential conductance is of molecular origin. The apparent gap and exponential turn-on of the differential conductance in the case of the BPE and BDMT suggest that adding localizing groups interferes with the conjugated aromatic system and suppresses the overall conductance through the molecule. This assertion is nicely demonstrated when comparing the BPE with the BPD molecule, where the addition of an oxygen atom between the conjugated rings suppresses the conductance almost entirely below 1V. A similar effect takes place in the BDMT dimers where the

methylene groups suppress the overlap of the molecular backbone orbitals with the contacts; one should take notice that the BDMT molecule is smaller that the BPD, so that the difference cannot be explained as a simple difference in tunneling distance. The BPE molecules give consistently lower conductance values than the BDMT; this may be an indication that the presence of localization centers in the molecule affects transport more than the reduction of the overlap with the leads; however the other differences between the two molecules are too big to make any firm conclusions on that ground.
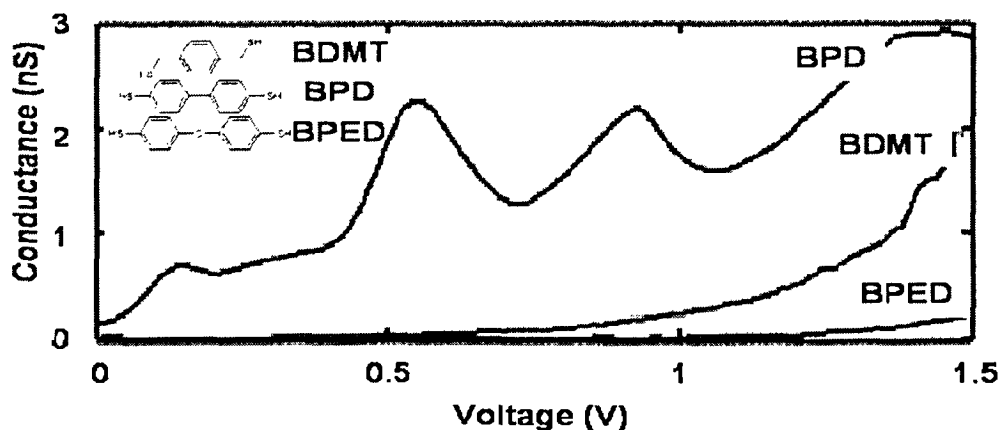

Figure 26 – Effect of conjugation on conductance

Typical curves of the three molecules; one can clearly see that at low voltages the conductance of the fully conjugated BPD molecule is much higher than that of the other molecules. The BPD molecule also has pronounced peaks in its G-V curve. The inset shows an illustration of the chemical structure of the molecules.

The conduction of these molecules was recently calculated theoretically using the greens function method [69] and the order of the conductance values of the molecules was reproduced (shown in figure 26). On the other hand the peaks in this calculation are spread significantly more than in the measurements.
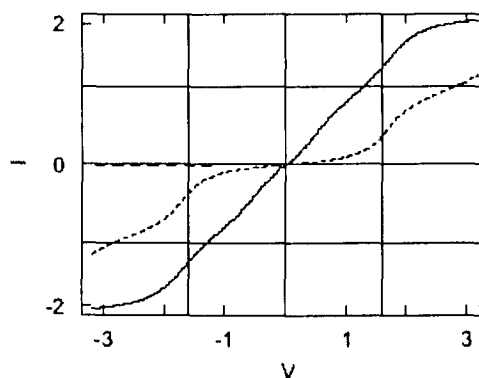

Figure 25 – Calculation of conductance values.

NEGF calculations of I-V curves for BPD (solid line), BDMT (dotted) and BPED (dashed), from reference 69. The units used are of e=h=c=1, meaning that the current is in the range of $10^{-7}A$, about an order of magnitude higher than that typically observed in our measurements.

52

The structure of the BPD curves

The BPD measurements clearly show a series of conductance peaks. These peaks cannot be attributed to charging of the gold nanoparticles – their typical spacing is a few hundred mV, more than an order of magnitude larger than the gold nanoparticles' charging energy. The peak structure typically appears on top of a rise in the conductance; this rise is very different from sample to sample sometimes differing by an order of magnitude, and changing from a strong exponential rise in some samples (figure 27a) to a moderate super-linear rise in others (figure 27b) and in one sample no background rise at all (figure 27c). A possible explanation for the existence of a background can be the existence of a resonant tunneling state above the range of the voltage window observed by the measurement; the variability between the different samples would mean that this state should be in different energies from one sample to the other. In light of the sample to sample difference it is probably most likely that the rise is

Figure 27 – different background rises in BPD samples. (a) A strong exponential rise. (b) A superlinear moderate rise. (c) No background rise.

connected to direct tunneling between the particles and therefore differs from sample to sample due to geometric differences amongst the samples. Most samples observed displayed a rise close to the moderate superlinear one shown in figure 27b, with two showing the strong exponential behavior and one displaying no background rise.

Another difference among the different samples is the width of the conduction peaks. Some samples display clear sharp peaks with well defined maxima and sharp rises and falls (figure 28a). Other samples have broad peaks that clearly mark some kind of resonance in transport, but are broadened out much more (figure 28b). This difference among the peaks found in different samples is probably a result of differences in the
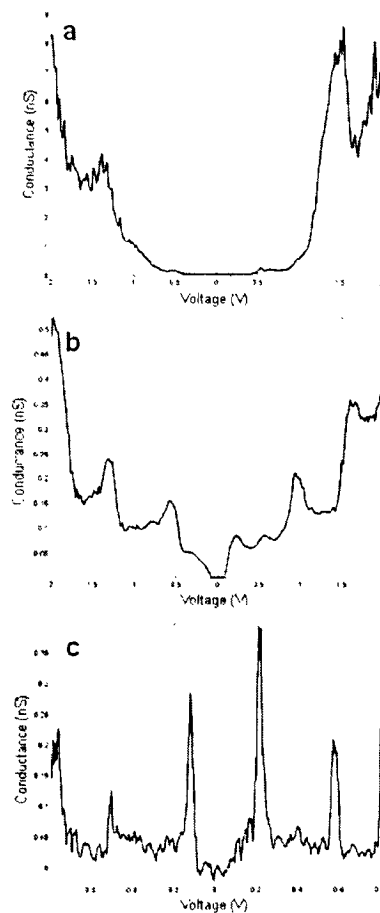
strength of the connection between the molecule and the leads, leading to a different broadening of the molecular levels, as discussed in the introduction. There is no correlation between the behavior of the background conductance and the shape of the peaks; this is consistent with the assumption that this rise is a result of inter-particle tunneling and not the electrical properties of the molecule. As can be seen in figure 28 there is also no correspondence between the overall conductance of the junction and the broadening of the peaks, this is strange since the connection to the leads should affect conductance. One possible explanation is that for the conjugated BPD molecule the junction conductance is limited not by the molecule but by the tunneling barriers formed by the ligands on the nanoparticles. This would mean that the conductance values found for BPD are in fact lower limits to the "real" conductance of the BPD molecule.
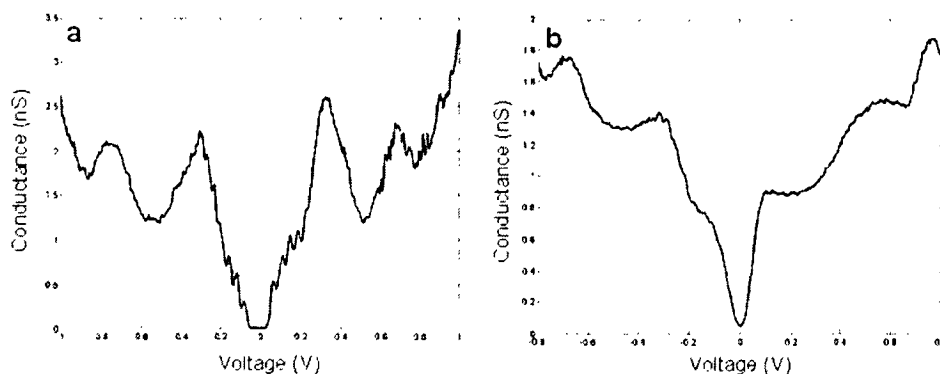

Figure 28 – different Peak shapes of the BPD molecule. (a) A sample displaying strong pronounced conductance peaks. (b) A sample with broadening of the peak structure. Nothe that both samples have approximately the same background rise and roughly the same overall conductance.

Random gating of the molecules

Another factor causing irreproducibility in the BPD measurements is the existence of temporal fluctuations as well as variations between different devices. Figure 29a shows a compilation of 130 measurements of the conductance of one dimer taken over a period of a few hours. Strong temporal fluctuations in peak position, which could be as large as a few hundreds of mV, are evident. We find that the conductance spectrum shifts rigidly, namely – all peaks at positive and negative voltages move to the same direction by approximately the same value. This is demonstrated in figure

29b, where we shift all spectra such that their peaks at -0.2V coincide. It is seen that this operation causes all other peaks to be aligned as well. Such behavior is typical of electrostatically gated Coulomb blockaded systems with different input and exit capacitances [11]. Plotting the conductance in the V_{ds}-V_g plane one obtains a skewed diamonds structure. It can be seen that under these conditions the conductance peaks at positive and negative drain-source bias indeed move rigidly upon application of a gate voltage. Since the gold nanoparticles are very effective in screening the effect of remote potentials we conclude that charge movement in close vicinity to the molecule gives rise to the observed rigid shift of the spectrum. These temporal fluctuations can therefore be considered as evidence for gating of the molecule, which occurs randomly. We note that the temporal frequency of this random gating depends on the voltage sweep rate, dV/dt, and the voltage range of the measurement. It could be substantially minimized by working at low sweep rates and within a limited voltage range, such that stable and reproducible measurements can be conducted over hours, as can be seen in the measurement of figure 29c.
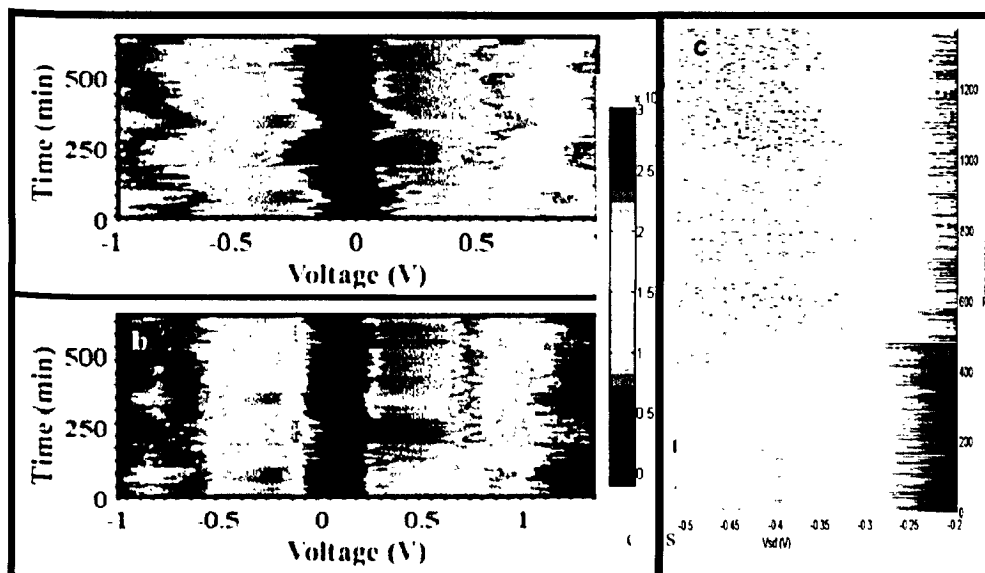

Figure 29 – random gating of the molecules. (a) A compilation of 130 measurements of the differential conductance spectrum of one BPD dimer, taken over a period of a few hours. The conductance values are represented by a color scale, which ranges from blue (0 nS) to red (3 nS). (b) The spectra of a shifted such that their peaks at 20.2V coincide, thus demonstrating the rigid shift nature of the temporal fluctuations. (c) A slow measurement with 1mV step size, of the peak at -300mV. Over the measurement period of 24 hours there was only one jump in the position of the peak.

positions (Figure 30). This is done by converting each spectrum to a set of peaks, each represented by a block of unit height, a width which is the full width at half maximum, and is centered on its maximum. A rigid shift of each spectrum was allowed to accommodate the temporal fluctuations. It is seen that the peak structure survives the averaging over many molecules, indicating that the variability in peak position is smaller than the peak spacing. The peak positions determined from the histogram agree very well with measurements done on self assembled monolayers of BPD [74] (see inset to figure 30). However, such agreement is lacking when comparing the measured spectra with recent calculations of molecular conduction [73]. In particular, the measured turn-on voltage is significantly lower than theoretically predicted. Moreover, the predicted conductance is much higher than that found in the measurements.
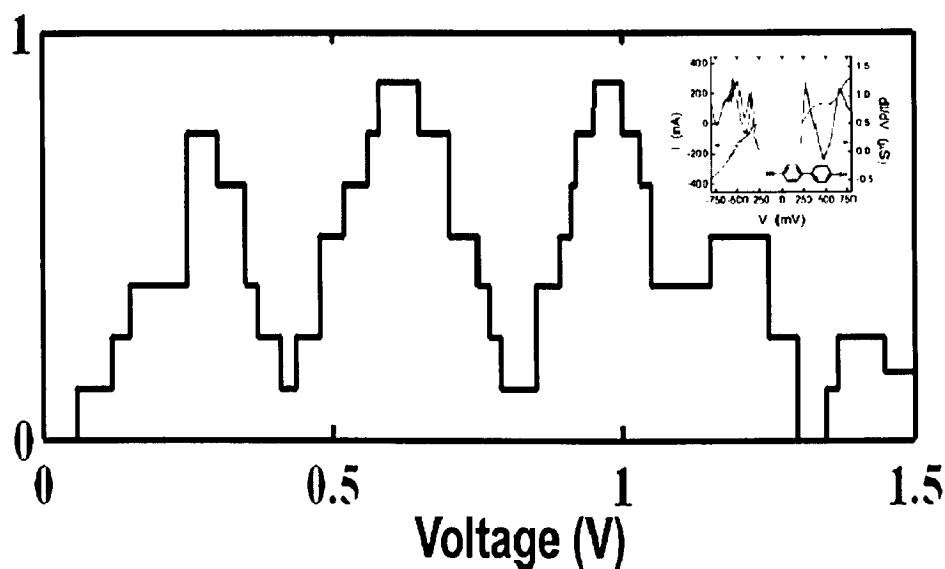

Figure 30 – Conductance histogram.

Histogram of the conductance peak positions collected from 15 BPD devices. A rigid shift of the spectrum by up to 50 mV was allowed. The inset shows measurements of SAMs of BPD molecules taken from 74.

Temperature dependence

Our measurement system creates single molecular junctions that are much more stable than those made by most other systems used today; this allows us not only to perform many repetitive scans at low temperatures, but also to measure the temperature dependence of the molecular conductivity in a well controlled way.

The temperature dependence of the BDMT molecule was studied first, with results shown in figure 31a. The temperature dependence data is reminiscent of the results reported by Selzer et.al. [35], yielding an excitation energy of approximately 50meV with applied voltage of up to 150mV. In the case of the BDMT there is no clear internal degree of freedom to associate with this energy scale as in the OPE of reference 35. The 50mV could involve motion of the molecular center of mass. Surprisingly, too, the energy gap calculated from this measurement remains unchanged up to a source drain voltage three times the size of the calculated gap, without a sginificant change of the Arrhenius plots found. This leads us to suspect a different explanation to these results, attributing them not to actual temperature dependence of the molecular conduction, but to thermal expansion of the electrode chip. At the temperatures studied, below 150K, the thermal expansion of the silicon substrate is negligible compared to that of the gold electrodes and nanoparticles [70,71]; thus heating will cause the electrodes to expand over the substrate and move closer. If we assume from the nonlinear G-V curve of BDMT that the molecule serves as a tunnel barrier between the leads this expansion will lead to an increase in the current. The
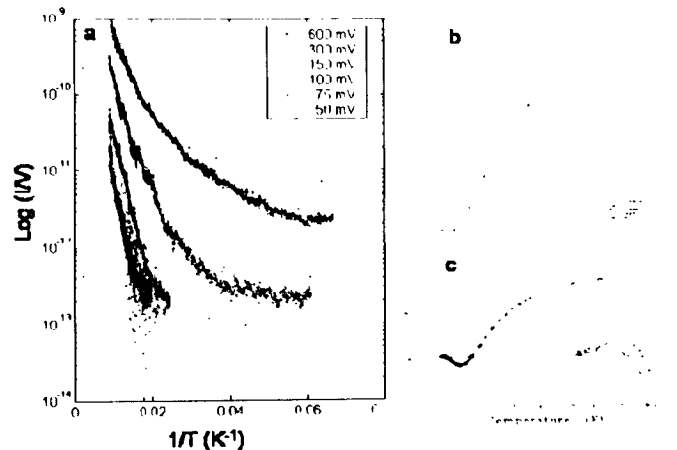

Figure 31: Temperature dependence of the BDMT molecular juntion conductance. (a) Arrhenius plots of the logarithm of the current as function of the inverse temperature. The low voltage data was taken only down to 50K, since at this temperature the measurement reached the noise level (b) Temperature dependence of the thermal expansion coefficient of gold. Taken from [71]. (c) Temperature dependence of the thermal expansion coefficient of silicon. Taken from [70].

thermal coefficient of gold begins to rise strongly near 50K (figure 31b), this can serve as an explanation to the lack of temperature dependence below that temperature. In the case of the BPD molecule the temperature dependence is much more complicated. We studied the effect of temperature both on the position of the different peaks, and on their shape. As can be seen in figure 32 the peaks appear at different source drain voltage values (different energies) at different temperatures, the shift of peak energies as function of temperature is usually quite gradual. The temperature dependence is repeatable during several cooling cycles, and therefore clearly a real property of the junction. When comparing the temperature dependence for different devices we find that the behavior is device specific, giving completely different results for each device. The temperature dependence of the peaks in the BPD dimers is therefore not a direct property of the molecule. One possible explanation to this strange device specific behavior is the same thermal expansion suggested previously for the BDMT measurements. In the BPD molecule the angle between the two phenyl rings has a very strong influence on the current, changes in the pressure applied to the molecule or shifting of the gold particles may cause this angle to change. Since the geometry of each device is different due to the random placement of the dimer thermal expansion may cause different changes in each molecule, thus leading to this device specific behavior.
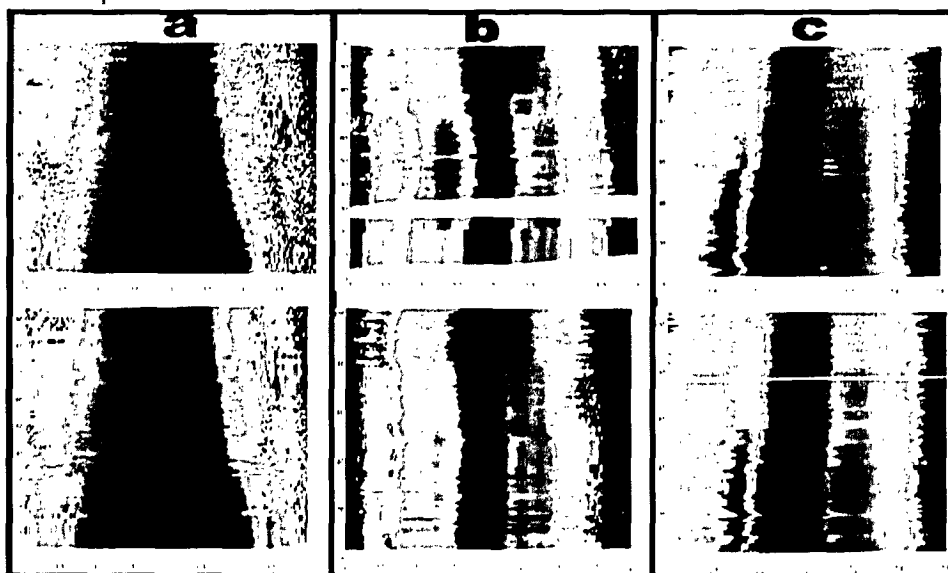

Figure 32 – Temperature dependence of the BPD conductance peaks

a-c) Repeated scans of different BPD molecules. Red/blue represent high/low conductance, respectively. The maximum ranges from 10nS in the left plot to 1 in the middle and right ones. The temperature dependence of the peak position is the same for each individual device, but it is very different from one device to the other.

While the effect of temperature on the position of the peaks is difficult to interpret, there is value to studying the change in the shape of the peak as function of temperature. We study the shape of the peak itself by removing a straight line from the plot and studying the peak without its background. Assuming that the peak changes only as a result of thermal broadening of the leads' Fermi function the transmission peak is expected to increase in width linearly with temperature and decrease in height linearly with the inverse temperature, so as to preserve the area under the peak [72]. It is evident that the peak broadens slightly and decreases in height with increasing temperature (figure 33). Surprisingly we find that the value of the conductance at the peak maximum does not decrease as $1/T$, but rather it decreases linearly with temperature as $G_{max} = G_0 - \beta T$.

The linear dependence of the peak maximum on temperature cannot be explained by the thermal broadening of the Fermi distribution of the leads. We would like to suggest a different mechanism for the peak lowering, based on the angle between the two phenyl rings. The phenyl rings are set at an angle φ_0 between them caused by the competition between the conjugation energy of the molecular π electrons and the steric hindrance of the hydrogen atoms. As the temperature increases the rings oscillate around this angle, changing the coupling of the π electrons on each ring. Calculations of the energy barriers for the twisting of the phenyl rings give an energy scale of a few kcal/mol for the difference between the steady state angle and the extremes of $0°$ and $90°$ [72]. Taking these values as estimates for the rotation energy in the bound single molecule we find an energy of a few eV per molecule. The temperature at which we are measuring is equivalent to about 10^{-4} eV, much lower than that of the barrier, so that we are able to assume small oscillations around the stable angle. The amplitude of a harmonic oscillator is proportional to the root of its energy, so we take the angle to be $\varphi = \beta\sqrt{T}\sin\omega t$, with β a small parameter. Making use of the $\cos^2(\varphi)$ dependence of the conduction, Taylor expanding the cosine by β and leaving only terms up to β^2 we get-

$$G \propto \int_{-\pi}^{\pi} \cos^2(\varphi_0 + \beta\sqrt{T}\sin t)dt \approx 2\pi\cos^2(\varphi_0) + (\sin^2(\varphi_0) - \cos^2(\varphi_0))\pi\beta^2 T$$

For the value of $\varphi_0 = 34°$ given in the literature [51] the second term gives a negative value of approximately -0.28, causing the observed linear lowering of the peak maximum. This result is very interesting because it not only provides us with a model

59

for the linear lowering of the peak maximum, it also gives us the prediction that if the steady state angle between the rings will be larger than $45°$, as for example is the case for fluorine substituted BPD ($\varphi_0 \sim 52°$), the trend should be reversed giving a rise of the peak with increased temperature. This prediction will be tested in future work done in our lab.

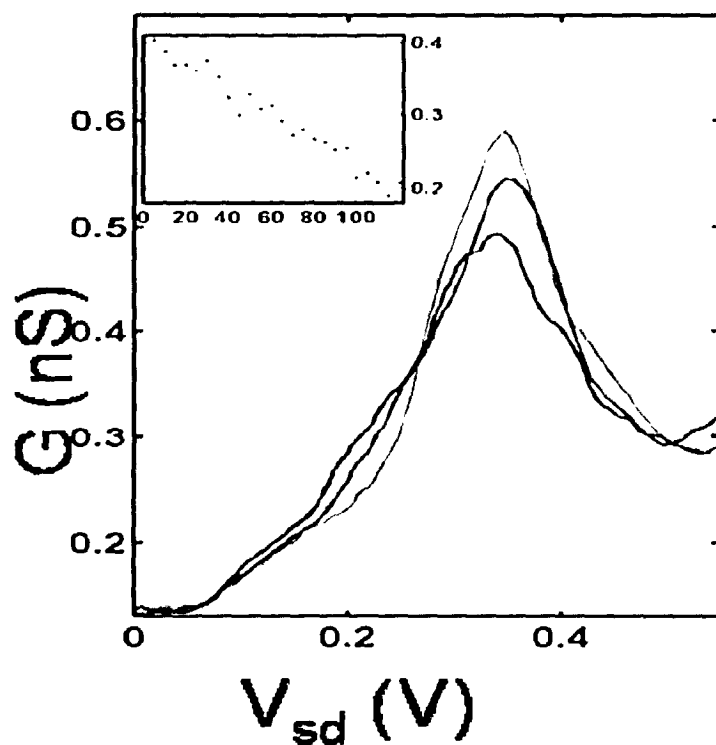Figure 33 – **Temperature dependence of the peak shape.** The shape of the peak as a function of temperature from 4K (cyan) to 80K (pink). The inset shows the peak height as measured with respect to a straight line connecting both sides of the peak

The importance of gating

Most measurements of molecular conductance spectra are based on scans of source drain voltage, without the ability to gate the molecule. If we assume that the peaks are electrostatic in nature, these measurements are essentially cuts in a two dimensional Coulomb blockade (CB) diamond plot of the system at some uncontrolled gate voltage imposed by the random environment. This will vary greatly from one measurement to the other, depending on the gate voltage and the coupling of the molecule to the left and right contacts. What one

Figure 34: Line scans in the CB diamond plot.

ΔE is the energy spacing that we would want to measure. As can be seen these cannot be found from the Vas scans without further information. a) Symmetric diamonds b) Vsd scans along the lines in fig 29a c) Skewed diamonds d) Vsd scans along the lines in fig 29c.

would like to obtain from these measurements is the value of the energy spacing ΔE of the levels thus measured. As illustrated in figure 34 this cannot be done with simple Vsd scans. The peak spacing taken from source drain scans like the ones illustrated in figure 34c and 34d can be different between different pairs of peaks, it can equal $2\Delta E$ as in the red graph of figure 34b, ΔE as in the two peaks nearest to Vsd=0 in the yellow graph of figure 34d or any other value less than $2\Delta E$.

One may ask, given this analysis, how we were able to acquire the histogram of figure 30. A possible explanation to that may be hinted by the random gating in figure 29. That data shows that the molecules tend to behave like strongly skewed CB systems, perhaps due to an asymmetry in the placing of the dimers on the electrodes. If the ratios of the capacitances are not very different from one device to the other we can expect to have a reasonably reproducible spectrum. It would however be impossible to assign the scale of the peak spacing to any physical property of the molecule without the knowledge of the capacitances that can be found only from a full two dimensional scan.

Thus it is clear that gating of molecules is necessary not only as a technological step, towards the creation of a molecular transistor, but also crucial in order to obtain quantitative information on the energy spacing of the molecular levels.
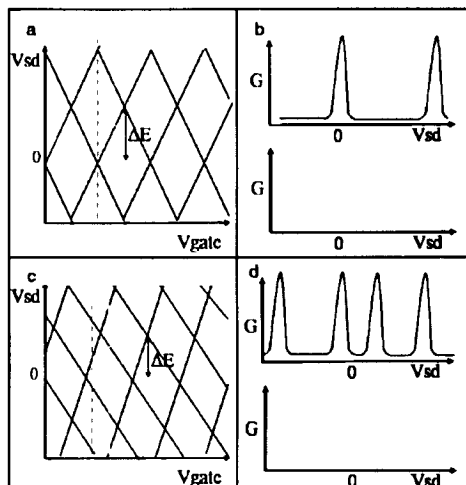
The problem in obtaining molecular junctions with significant gate response is common to all single molecule measurement systems; it arises from the difficulty in affecting the electrostatic environment in a nm sized gap screened by two large metallic electrodes. The potential between the electrodes can be shown, in the simplified model shown in the inset of figure 35, to decay very rapidly with the height as $\Phi\sim\exp(-h/d)$, where h is the height of the area between the electrodes, and d the distance between them which is dictated by the size of the molecule. One should notice that h here refers to the height of the area enclosed between the metallic electrodes, and not the total distance to the gate, making changes in the oxide thickness insignificant for the screening problem. As can be seen in figure 35 the height of the area where the electrode spacing is smallest in our
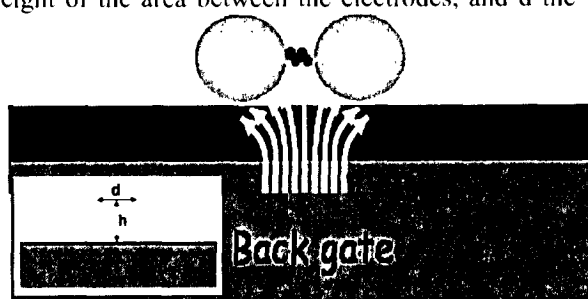

Figure 35: Screening of the back gate.

Field lines emerging from the back gate in a dimer measurement configuration. The most significant decay of field lines is between the particles. The inset shows a simplified model used to understand the dependence of the screening.

method is defined by the size of the nanoparticles used to form the dimer. We should therefore be able to improve our ability to gate the molecule by reducing the size of the particles as much as possible. By switching to nanoparticles with an average diameter of 15nm, who furthermore are single crystals, we have been able to obtain several molecular junctions, which display a response to the gate voltage. In the following section we will show and discuss each of these individually.

Molecular structure dependence of the peak structure

In order to interpret the peak structure of the molecular conductance we have fabricated dimers of four different molecules: the old BPD molecule, BDT (1,4 benzenedithiol), and both these molecules with fluorine substitution of the hydrogen in the benzene rings FBPD (4,4'-octafluorobiphenyldithiol) and FBDT (1,4 tetrafluorobenzenedithiol); References to the synthesis of these molecules can be found in appendix B. The rationale behind choosing these molecules was that by comparing BDT with the BPD
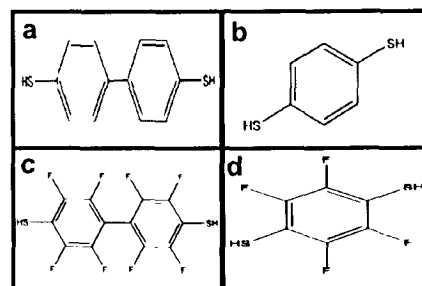

Figure 36: Molecular species investigated

Schematic illustration of the (a) BPD (b) BDT (c) FBPD and (d) FBDT molecules.

we would be able to observe effects relating to the molecule size. The fluorine substation is expected to have two significant effects: the vibration energy of the C-H atoms will be replaced by the smaller energy of C-F vibrations; more significantly the fluorine atoms, that have a much higher electronegativity than that of the hydrogen will attract electrons from the benzene rings, causing a change in the spatial distribution and energy of the molecular orbitals.

Out of seven BPD molecule, 5 FBPD, 5 BDT and one FBDT molecule we have been able to gate one each of the FBPD and BDT and two BPD molecules.

Starting for the measurement of the BDT molecule shown in figure 37, in this and in all the following figures we have subtracted a line of the background rise to enhance the peaks. The first thing that can be seen is that the molecular peaks indeed give rise to CB diamonds upon gating. This observation is not a trivial one; the formation of CB diamonds indicates that the features involve a process that is electrostatic in nature. If some other process such as vibration assisted tunneling were taking place we would have expected to see these peaks appear as parallel satellites to the CB peaks. Another feature that needs to be addressed is the fact that the diamonds at positive and negative bias do not close near zero Vsd. There is a strong low voltage gap, preventing the diamonds from closing and they are shifted one with respect to the other. This can perhaps be attributed to the presence of the nanoparticles (whose features can also be seen in the small oscillations at low Vsd); for current to go through the system a low bias both particles need to have a state near the electrodes' Fermi energy. Since the system has only one gate, the two particles can't be tuned perfectly, leading to an inability to close the gap completely. The issue of modeling this system completely, taking into account the particles as well as the molecule is currently being studied in our group by Avraham Guttman. The spacing of the energy levels of the molecule is taken as half the distance in source drain voltage between two diamond vertices.

Figure 37: CB diamond measurements of BDT molecule.
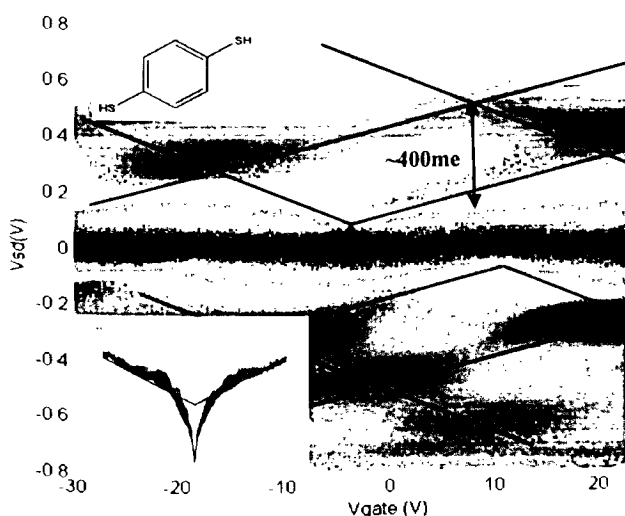Conductance as function of bias and gate voltage, red/blue indicate high/low conductance respectively. Values of conductance are arbitrary due to the line subtracted from the measurement, which is shown in the bottom inset. Black lines are guides to the eye, the lower lines are the top ones reversed and shifted. The top inset shows the chemical composition of the BDT molecule.

Figure 38 shows a diamond diagram of the FBPD molecule. The diamond structures in figure 38 have a smaller gap at low bias, and are not shifted; this is probably due to some difference in the geometry of the device.
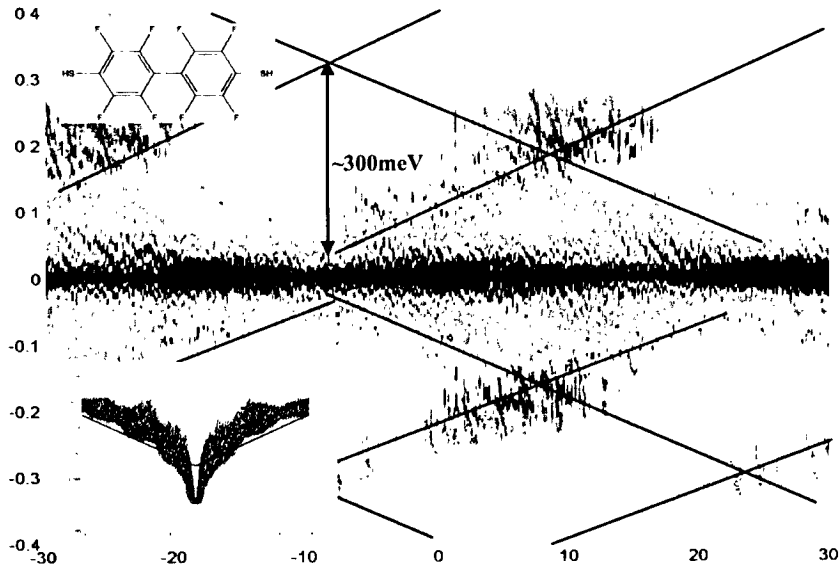

Figure 38: Coulomb blockade diamond measurements of the FBPD molecule.
The details of this figure are the same as in figure 31. The beating created by the two nanoparticles can be seen as nearly vertical lines

in the scan. Naïvely this beating can be understood as a result of the alignment of the energy levels of the two dots, as shown in figure 39. A slight difference in the size of the dots will cause them to have slightly different charging energies. When the states in both dots appear at the same energy there is a high conductance through the system, while when there is a mismatch there is a reduction in the conductance. The gate will also have a different effect on the two particles, due to the random placing of the dimer in the gap. This will cause the beat pattern to respond to the gate voltage as seen in figure 38. Both these features can be explained in a more complete way using the theory of two quantum dots connected in series [75], this will be done in the next section.
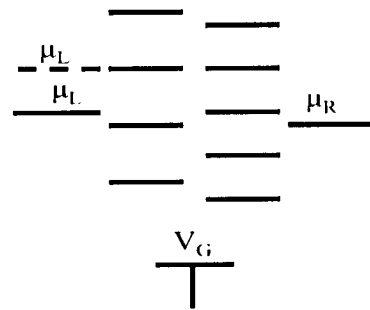

Figure 39: Schematic illustration of the two dot system, with the molecule as a tunnel barrier. The solid line represents a state of the system with lower conductance compared to the dashed one, where the two ladders coincide and the conductance is enhanced.

Turning now to the measurements of the BPD molecule, we have two measured devices. The first device shown in figure 40a displays behavior more or less like that of the other molecules. There is a low bias gap and the beating of the two dots can be observed. The second device, shown in figure 40b displayed very different behavior. This device had no background rise in the conductance giving a conductance of nearly zero everywhere except at the position of the peaks (see inset to figure 40b). Only one set of peaks could be observed, typical to a case of a quantum dot were one tunnel junction has a much higher resistance than the next (see next section). The overall current in this device was also extremely low. We tend therefore to assume that the device of figure 40b was anomalous in one of the connections to the molecule, perhaps with the molecule connected in a different configuration than is normal. The different connection to one lead will clearly change the electronic states of the molecule, thus making it difficult to compare this device with the other ones.
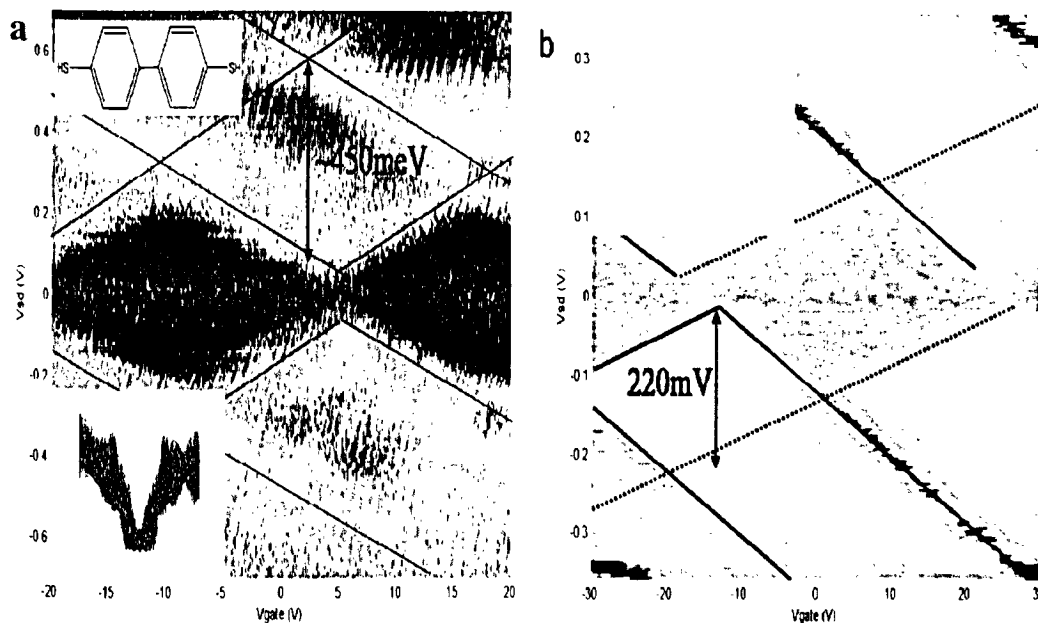

Figure 40: Coulomb blockade diamond measurements of the BPD molecule.

(a) a "normal" BPD device with symmetrical diamonds. (b) An "abnormal" device with no background rise and only one set of peaks. No background was removed in this plot. The inset shows a G-V scan at zero gate voltage of the device.

From the CB diamond plots we are able to assess the energy level spacing of the molecules. We find the highest level spacing in the "normal" BPD molecule (225meV) then the BDT (200meV) and finally the FBPD (150meV). Clearly, in light of the two very different BPD measurements, without repeated measurements we cannot assume that any of these results are really specific to the type of molecule studied and not device specific. To answer that we would need significantly more data on all four molecules that we attempted to study, and also a better way of modeling the system that would include not only the molecules but also the particles connected to them in the analysis.

Double dot physics

While the declared goal of this work is to study the properties of the molecules in our junctions, we have seen already in the previous results that the gold nanoparticles too play a role in affecting the transport properties of our junctions. This can allow us both to make use of the nanoparticle physics in characterizing our system, and to study the double dot phenomena that appear. Figure 41 illustrates the different possible approaches to modeling the transport through the dimer, considering the molecule as a third quantum dot (option II) as we did so far, or as a featureless tunnel barrier (option1). In the study of the part played by the nanoparticles in our system we use the modeling of option I; this is appropriate in the region of source drain voltage below the appearance of the first molecular peaks, or in cases where the molecular peaks do not appear at all. Under this assumption the system can be described as two metallic quantum dots connected in series, and the physics we expect to observe is that of double quantum dot (DQD) systems [75].
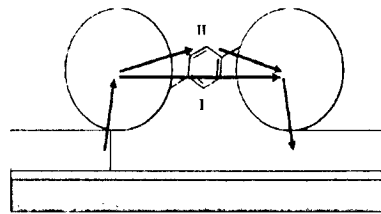

Figure 41: The possible ways to treat the molecular junction. Pathway I treats the molecule as a featureless tunnel barrier, while II describes a situation where the electron dwells on the molecule during transport.

The subject of two quantum dots (QD) connected in series has received much interest in recent years, due the possibility of applying it to the field of quantum computation [77]. These works tend to focus on GaAs QDs, which are easier to fabricate and control, and on the properties of these systems at zero bias. Some work has also been done on the properties of metallic dots at finite source drain voltage [78,79]. Lithographically defined QDs are two dimensional and are affected by two different energy scales, the level spacing and the charging energy, both in the range of 1meV or less while in metallic QDs the only relevant energy scale is that of the dot charging energy, in our system 40-50meV. Metallic dot systems are also different in the fact that they have many free electrons in them compared to GaAs ones, where there is the possibility to completely tune the number of electrons in the dot. There is much value therefore to the study of the two metal nanoparticle system individually; this will be the focus of another PhD. done in our group. For the purpose of this work the focus on the double dot physics is only from the aspect of the information that may be

gained from them on the molecular junction. A full description of our system in terms of double dot physics should enable us to assign the capacitance and resistance of each junction in it, and to know the voltage division along the dimer. This will allow us to answer the extremely important question of how much voltage is actually applied to the molecule, and how much drops at the electrode-particle contact. Since the electronic orbitals of the molecule are expected to react to the applied voltage, and thus change the transport properties of the molecule [17] this is clearly an important question to address.

Theoretical description

The theoretical work done on double quantum dot (DQD) systems has focused mainly on the aspects relevant to the experiments done in GaAs heterojunctions for the purpose of quantum computaion. The study of these systems is somewhat different from the work we are doing; in heterojunction DQDs one usually focuses on the properties of the system at zero applied bias, using two separate gates to control the state of the dots individually. The focus is not so much on the transport through the system, but rather on the state of the electrons in the dots. The theoretical understanding of these systems is, however quite exhaustive [76] and can be applied to the dimer system as well.

The state of the system is found by calculating its energy dependence on the charge states of the two dots, neglecting any cross capacitance terms this energy is given by

$$U = \frac{1}{2}N_1^2 E_{C1} + \frac{1}{2}N_2^2 E_{C2} + N_1 N_2 E_{Cm} + f(V_{g1}, V_{g2})$$

where $E_{C1(2)}$ is the charging energy of dot 1(2), E_{Cm} is the electrostatic coupling energy of the two dots, and f the gate influence:

$$f = \frac{1}{e}\{C_{g1}V_{g1}(N_1 E_{C1} + N_2 E_{Cm}) + C_{g2}V_{g2}(N_1 E_{Cm} + N_2 E_{C2})\} + \frac{1}{e^2}\{\frac{1}{2}C_{g1}^2 V_{g1}^2 E_{C1} + \frac{1}{2}C_{g2}^2 V_{g2}^2 E_{C2} + C_{g1}V_{g1}C_{g2}V_{g2}E_{Cm}\}$$

from this one defines the electrochemical potentials of the dots as the energy needed to add the $N_{1(2)}$th electron to dot 1(2) while there are $N_{2(1)}$ electrons on dot 2(1):

$$\mu_{1(2)}(N_1, N_2) = (N_{1(2)} - \frac{1}{2})E_{C1(2)} + N_{2(1)}E_{Cm} + \frac{1}{e}(C_{g1}V_{g1}E_{C1(Cm)} + C_{g2}V_{g2}E_{Cm(C2)}).$$

From these potentials one can find the number of electrons on the dot, by requiring that each dot has the maximal number of electrons on it, such that its potential is lower than that of the leads (set to 0). This information is summarized in the charge stability diagram (or honeycomb diagram) as shown in figure 42, in which hexagonal

domains signify areas in which there is a specific charge configuration in the system.

The shape of the honeycomb diagram reflects the different parameters of the DQD system. In the case of completely decoupled dots the domains are squares parallel to the gate voltage axes, with the charge on each dot essentially controlled only by one of the gates (figure 42a). If the coupling is increased the lines in the diagram obtain a slope and the vertices split into "triple points" (figure 42b). These are connected by a line signifying a jump of a single electron from one dot to the other due to this coupling. Increasing the coupling further causes the triple points to separate further and the DQD system behaves like a single dot with N_1+N_2 electrons on it. The triple points are very important in the analysis of transport through the system, since they are the only spots on the diagram where transport can occur at zero bias. Transport is obtained by the consecutive tunneling of an electron or hole from one lead to the first dot, between the two dots, and out to the next lead, therefore it requires that the three intermediate charge states be degenerate.

Figure 42 Different honeycomb diagrams. Charging states of the dots are denoted in parentheses in each domain. (a) No intradot coupling, two separate sets of charging of the dots. (b) Intermediate coupling, yielding a honeycomb shape. (c) Large coupling, the two dots behave like a single dot. (d) Detail of the dotted square in (b) showing the triple points, and the order of transport through the system.

The honeycomb diagram describes the response of the system at zero bias to two different gates, coupled mainly to one dot each. Our system is different, since we have only one gate. The back gate is coupled to both dots, but with slightly different capacitances, so that a gate scan in this system is essentially running along a diagonal line in the honeycomb, randomly oriented based on the specific system geometry. This observation can serve to explain the gap appearing in our measurements at zero bias (figures 37, 38 and 40), and the different size of this gap in each measurement. For a complete closing of the gap at zero bias the diagonal must coincide exactly with a triple point, the chances for that are negligibly small but for each orientation the bias necessary for the onset of conduction will change.
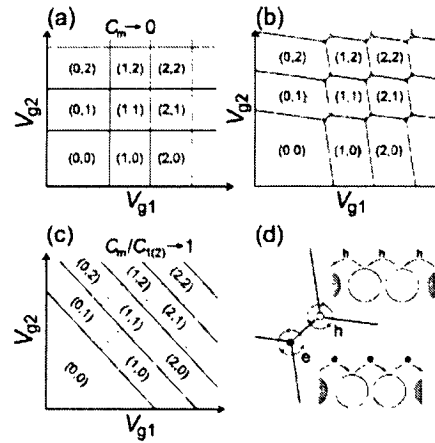
At higher bias the triple points of figure 42 change, turning into triangles, bounding the area in the V_{g1}-V_{g2} plane in which the electrochemical potentials of both dots are between those of the leads (shown in figure 43). At some finite bias these triangles will intersect with the gate scan line, and current can begin to flow. The appearance of the triangles at finite source drain voltage provides a more detailed explanation of the beating observed in the previous section. The triangles increase linearly with the bias creating three sets of parallel lines that intersect with the point the system is placed at and create conductance peaks. The conductance can then be expressed as a sum of cosines which can be expressed as a multiplication of cosines with frequencies of the average and difference of the original frequencies. If the frequencies are close to one another this will cause
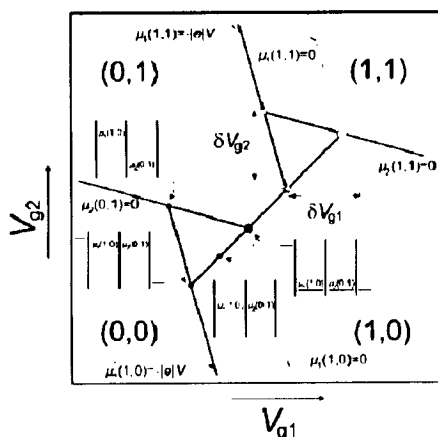

Figure 44: Triple points at finite bias. The vertices of the triangles mark the points where the states of the dots coincide with the electrochemical potential of the leads.

Figure 43: The beat.

(a) A measurement of a dimer showing the beating of the conductance peaks. Red/blue signify high/low conductance. The yellow line shows the response of the beat to the gate and the black the "regular peaks". (b) A line scan at zero gate voltage showing the beat.

the peaks to appear as fast oscillations with a slow beat, as seen in figure 44b. The beat will also respond to the influence of the gate, but with a different angle than the regular peaks (figure 44a).

DQD physics in dimers

In some samples we encounter cases where the dimers do not exhibit the high energy molecular features. We interpret this to mean that the molecule in this case does not take an active part in the conduction, this could be due to some damage caused to it,

or simply because the particles are very close at some other point, making regular tunneling through the citrates the better transport mechanism. In these samples the low voltage behavior is not obscured by the high voltage one, and we are able to get clear double dot data reminiscent of the data presented in reference 78. These samples can be used as test cases to ascertain that our understanding of the DQD systems is good. A simulation for the DQD system using rate equations was written by Avraham Guttman, a PhD. Student in our group [80]. This simulation was used to study the measured DQD results and characterize the capacitances and resistances of the system. We find from the simulation that the shape of the DQD diamond plots is influenced only by the capacitances of the system. Resistance differences affect the relative strength (magnitude of conductance peak) of the relevant lines, sometimes causing them to disappear altogether.

The DQD measurements of dimers without high energy features and corresponding simulation results are shown in figure 45. The alternating large and small diamonds near low V_{sd} are a signature of the double dot physics governing the system. Large diamonds are a result of the energy spacing of the dots, while the smaller ones are a result of the electrostatic interaction between the two dots. Figure 45b and c show the features of the dimer shown in figure 45a; the capacitances of the dots to the leads are roughly similar, as seen from the symmetrical plot. The opening of the low voltage gap is a result of a difference in the capacitances of the two particles to the gate ($C_{g1}=1.4C_{g2}$), this may be because of a small size difference in the particles that may be seen in the SEM image; there is also a significant difference in the resistances of the particles ($R_1=3R_2$) leading to one set of lines being stronger than the other. The most striking feature in the measurement shown in figure 45e is the lack of one set of lines, this is a result of the different resistances of the particles to the leads ($R_2\approx70R_2$); this result is somewhat reminiscent of the BPD measurement of figure 40b, allowing us to assume that the molecule in that measurement was indeed connected badly on one side. As can be seen the model describes the system well and can provide a full description for it.
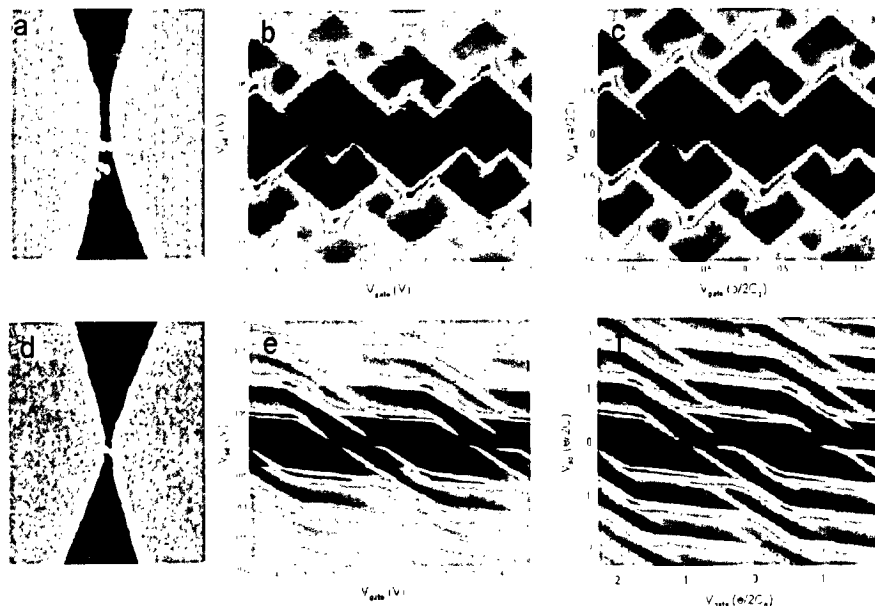
Figure 45: measurements of the low voltage features of the double dot structure.

(a-c) SEM image, measurement and simulation of dimer #1. A low voltage gap opens from 10 to 50 mV. The parameters of the simulation are: $R1-10R_0$ ($R_0-13MOhm$), $Rm-100R_0$, $R2-3R_0$, $Cg1-0.58aF$, $Cg2-0.44aF$, $C1-1.63aF$, $Cm-1.44aF$, $C2-1.86aF$ (the subscript one indicates the left particle, 2 the right one and m is the junction between the particles) (d-e) As in a-c for dimer #2. $R1-1.4R_0$, $Rm-1.8R_0$, $R2-100R_0$, $Cg1-0.12aF$, $Cg2-0.13aF$, $C1-2.15aF$, $Cm-1.57aF$, $C2-1.77aF$. In both measurements red is approximately 1nS and blue zero.

In a few of the samples we have measured one can observe the DQD features at the low voltage when there are also molecular features. Figure 46 shows a BDT device where the influence of the gate on the molecule was too small to create good gating but at low voltage one can see the DQD features of the dimer. The DQD features observed here are very noisy, but we should be able to reproduce them in the simulation. We can use this data to study the behavior of the molecule at low bias, in the range before its first conductance peak.

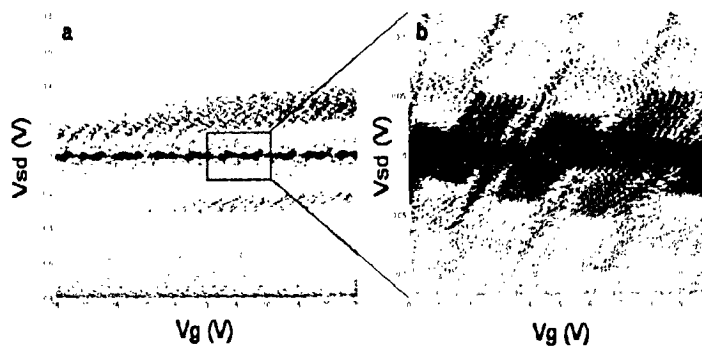**Figure 46: DQD and molecular features.**

(a) Scan showing high voltage molecular features and low voltage features arising from the DQD physics. Red is 2nS and blue zero (b) measurement of the low voltage features. Red is 1ns and blue zero.

72

Summary

This thesis has been a description of the work done during my PhD in realizing and utilizing the dimer method for single molecule conductance measurements. The dimer method provides the field with several advantages over other existing methods:

- Samples can be imaged in a SEM and by the presence and brightness of the nanoparticles one can have a clear indication of the existence of molecules in the junction, and the quality of the electrical contact to them.

- The ability to fabricate many of the constituents of the system using standard lithography and wet chemistry allows parallel processing for most of the process, enabling a greater yield than in break junction methods.

- Devices are stable for time periods on the order of weeks, and measurements on each device are reproducible after several cooling cycles; allowing many measurements to be made on each device.

- The modular character of the system allows use of nanoparticles from different materials with relative ease, enabling measurement of transport with two different metals on either end, or with semiconducting nanoparticles. This also allows control of each stage of the process individually providing better understanding of the system.

- Gating of the molecular junction is achievable in this system in a relatively straightforward way.

The method has several limitations:

- Molecules used need to have anchors located at their edges, making synthesis and availability of molecules a significant bottleneck.

- Despite the improvement in fabrication efficiency, obtaining working devices is still a difficult challenge, limiting the ability to obtain very large statistics.

- Full modeling of the nanoparticle-molecule-nanoparticle system is still necessary to understand the issues like the voltage drop across the junction and the low energy features appearing in the measurements.

We have used the dimer method to demonstrate the importance of electronic conjugation in obtaining a highly conducting molecular junction. We have identified peaks in the conductance of conjugated molecules, and shown that the peak structure in the case of the BPD molecule is reproducible from sample to sample. The stability of our samples has allowed us to track the temporal behavior of the peak structure, showing that the peaks are susceptible to random electrostatic gating. Study of the temperature dependence of the peak structure has demonstrated that the temperature influence on peak positions is sample dependent, but study of the shape of the peaks indicates that the temperature dependence of the peak height is dominated by the

amplitude of rotations between the two phenyl rings around their steady state angle.

We have demonstrated gating of three different molecules showing that the peaks respond to the gate, forming large scale Coulomb diamonds; we take that as an indication that the peaks represent charging states of the extended molecule. We have not been able to assemble enough data to demonstrate dependence of the CB diamond plot on the molecular species used, but that issue will be addressed in future studies. The peaks and their energy scale of a few hundreds of mV are extremely interesting and should certainly attract more attention in future work. While the gate response seems to indicate that the peaks represent charge states, the energy scale of the peaks does not fit with the theoretically predicted charging energies (on the eV scale). More work needs to be done studying this peak spectrum on different types of molecules, perhaps with a stress on synthesis to create molecules which will have different charging energies (large polyacenes may have significantly lower charging energies), and it should be possible to assemble a full description of the origin of these peaks.

Another line of study opened up by the dimer method is that of two metallic dots connected in series. The dimer method is ideal for the study of this system, allowing easy changing of the dot material, control of the contacts via the SEM etc. This work will be continued in our lab by Avraham Guttman.

While the dimer method is not an "ultimate" method to molecular measurement, it provides many significant benefits. It is probably better than the other existing methods in creating reliable, well characterized and stable molecular junctions. I would claim that a combination of the dimer method for long measurements including gating and thermal cycling, in conjunction with the histogram method to provide statistically significant data regarding the low voltage molecular transport behavior should supply future research in the field with the best data available.

Appendix A – Preparation of the gold nanoparticles

10-18 nm Au particles

A solution containing 1 ml of 1% NaAuCl$_4$, in 79 ml of DDW (solution A) and a solution containing 4 ml of 1% Na$_3$citrate, 16 ml of DDW, and 1% Tannic acid (solution B) were each heated to 6 0 °C [55]. Then solution A was added to solution B while stirring. The solution was slowly brought to a boil, exhibiting a shift to a red color, kept at 100 °C for 10 minutes, and then cooled to room temperature and stored in dark bottle at 4 °C.

The tannic acid promotes the formation of nucleation centers for the gold particles at 60 °C; these do not begin to grow till the temperature reaches 100 °C. Thus varying the amount of 1% tannic acid controls the size of the resulting particles, where more tannic acid yields more nucleation centers and smaller particles.

1% tannic acid	Large axis of resulting particles	Small axis of resulting particles	Color
50 µl of 3 nm seeds	11±1nm	10±1nm	Red
35 µl of 3 nm seeds	17±2nm	15±1.5nm	Red
20 µl of 3 nm seeds	19±2nm	17±2nm	Red

Au "Seed Nanoparticle" Solution

The Au nanoparticle seed solution is used as a basis for the creation of particles with a diameter larger than 30 nm. The solution is prepared by adding 1 ml of 1% aqueous HAuCl$_4$•3H$_2$O to 100 ml of H$_2$O while stirring [54]. One min later, 1 ml of 1% aqueous Na$_3$citrate was added followed, after another min, by 1 ml of NaBH$_4$ in 1% Na$_3$citrate. The solution is stirred for 5 min and stored in a dark bottle at 4 °C.

Larger Au particles

Particles with a diameter of 30nm and above are prepared using a two-step process, starting with a seed solution of small particles, which are increased to the desired size.
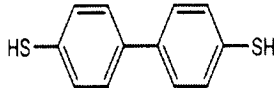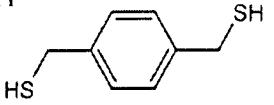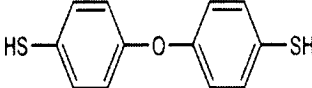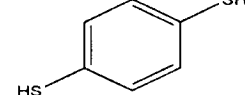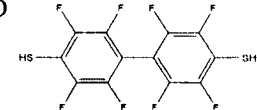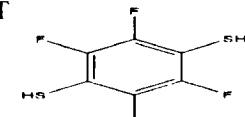
We have done this using both the 3nm and 10nm nanoparticles as seeds. We have found that the particles created from the 10 nm seeds have a better control of their size and are less elliptical.

Particles were prepared by adding 0.4 ml of 1% Na_3citrate and Au "seed nanoparticle" solution to 100 ml of a refluxing 0.01% aqueous solution of $HAuCl_4 \cdot 3H_2O$ while stirring. Refluxing was continued for about 15 min (or until a change of color was observed), the solution was cooled to room temperature and stored in a dark bottle at 4 °C.

The control of the particle size is achieved by changing the amount of seed solution added, where the more seeds are added the smaller the final resulting particles are.

Au seed solution	Large axis of resulting particles	Small axis of resulting particles	Color
65 μl of 3 nm seeds	35 ± 7 nm	26 ± 4 nm	Red
60 μl of 3 nm seeds	53.5 ±10 nm	40 ± 6 nm	Purple red
15 μl of 3 nm seeds	107±23 nm	64±13 nm	Orange
3.5 ml of 10 nm seeds	33±4 nm	30±2 nm	Red
1.5 ml of 10 nm seeds	57±6 nm	49±5 nm	Purple red

Appendix B – Molecules and the solvent used to dissolve them

Molecule	Solvent	Reference for synthesis
BPD HS—⬡—⬡—SH	NaOH 10M	81
BDMT (structure with SH and HS groups)	NaOH 10M	Available commercially from Sigma
BPED HS—⬡—O—⬡—SH	NaOH 10M	81
BDT (structure with SH and HS groups)	NaOH 10M	Available commercially from Sigma
FBPD (fluorinated biphenyl structure)	THF (Tetrahydrofuran) Acetonitrile	82
FBDT (fluorinated structure)	Acetonitrile	82

Appendix C – The gradient separation method

After formation of the dimers there are approximately 10% dimers in the solution. We wish to increase this percentage in order to improve the yield of our process; this is done by spinning the solution in a glycerol gradient. The gradient is prepared by mixing high and low density solutions of glycerol in a tube in a controlled way.

First the low density solution (typically 10%) is poured into a tube, and then the high density solution (45% for the small particles and 75% for the large ones) is carefully injected under it with a syringe so as not to cause any mixing of the two solutions. The tube is the rotated at a fixed angle in order to create a continuous density gradient along the tube.

After the gradient is prepared the dimer solution is added carefully to the top of the gradient tube. The solution should be added slowly while touching the pipette to the side of the tube; this serves to reduce the sinking of the solution in the gradient and improves the spread of the results.

Finally the tubes are placed on a Beckman SW-41 swinging bucket rotor in an ultra centrifuge and spun at a high velocity for several minutes. The spinning causes the nanoparticles in the solution to travel down the tube. The speed at which a particle travels is a result of the competition between the force it feels, which is proportional to its mass and the friction of the solution, proportional to its surface area. This causes the larger particles to travel faster due to their higher mass to surface ratio and reach a lower point in the tube. Typical centrifugation parameters for smaller particles are 15000RPM for 15 minutes in a 10-45% solution, and for the larger one 12000RPM for 12 minutes in a 10-75% solution. At the end of the centrifugation we allow the centrifuge to reach a full stop of its own accord, without use of the brakes, so as not to disturb the solution.
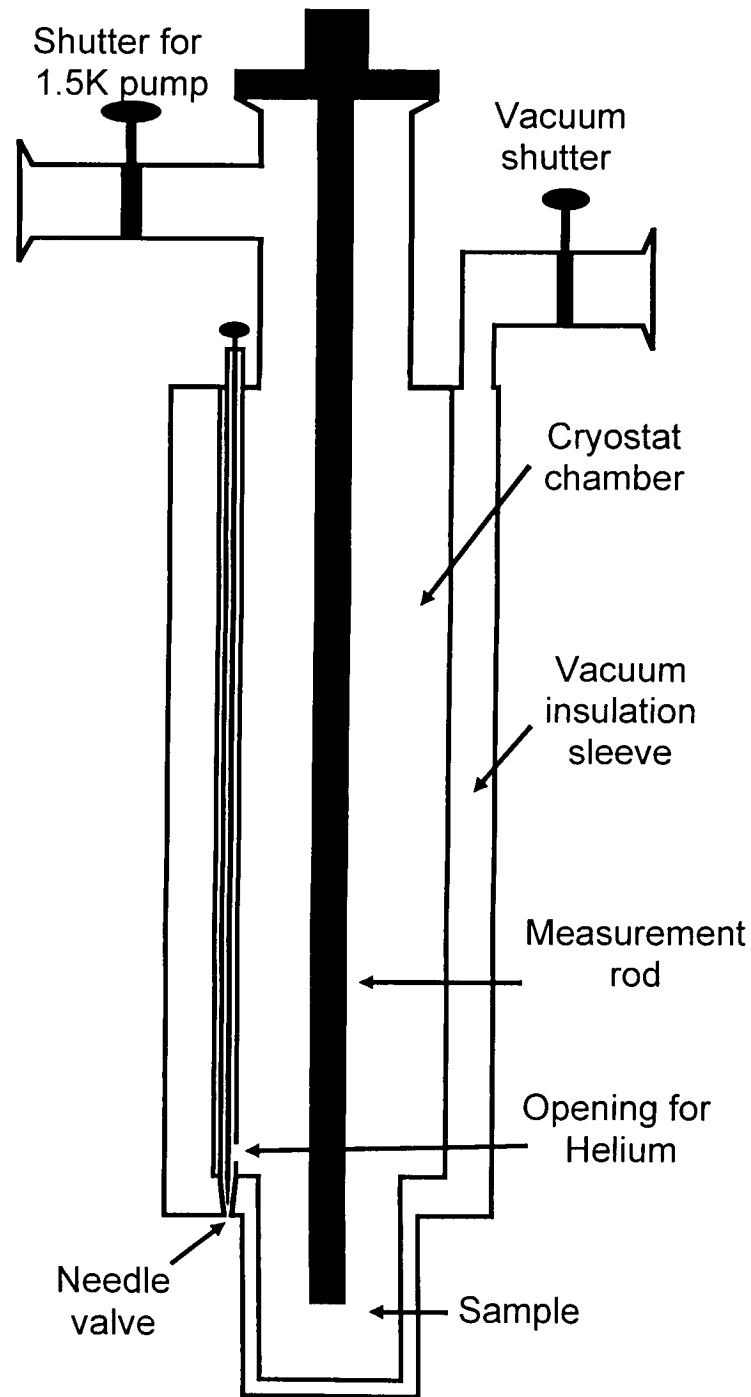
After centrifugation the tube is pierced at the bottom and the solution is extracted from it slowly by pumping 10% glycerol through its top at a rate of 1ml/min. The solution is divided into different fractions of 300µl each and kept at 4°C until they are ready to be used.

Appendix D - Fabrication of e-beam defined electrodes

A metal electrode system consisting of source and drain with a minimal gap of 25 nm was formed on a p-type Si substrate with 100 nm SiO_2 on top, using electron beam (e-beam) and optical lithography techniques. After applying a primer for adhesion of the resist to the SiO_2 (5,000 rpm, 60 sec, baked for 5 min at 80 °C) we apply a double-layer electron resist system consisting of PMMA 200K (5,000 rpm, 60 sec, baked for 1 hr at 180 °C) and PMMA 495K (8,000 rpm, 60 sec, baked for 1 hr at 180 °C) for resist patterning by e-beam writing. A 120 kV electron beam was irradiated on the resist system (Jeol JBX-9300 FS) and the irradiated resist was developed (1 min) using a 1:3 mixture ratio of MIBK (methyl isobutyl ketone) and isopropanol.

Subsequently, electron beam evaporation was carried out to form a layer of 7 nm Ni and 23 nm Au. The metal films were subsequently lifted-off by soaking the sample in acetone, rinsing it with isopropanol, and drying with nitrogen gas. The e-beam fabricated electrodes were connected to bonding pads defined by photolithography. Image reversal photo resist AZ5214E was used for patterning (spin coating 5,000 rpm, 40 sec, pre-baking at 100 °C for 1.5 min). The wafer and the contact pads' optical lithography mask was aligned and exposed to 415 nm light at 15 mW for 4 sec, then post-baking of 2 min and flood exposure of 1.5 min. The pattern was developed with AZ726 developer for 30 sec. The contact pads were fabricated by e-beam evaporation of a Ti (10 nm) adhesion layer followed by 200 nm Au layer and lift off. The electrodes were examined using a scanning electron microscope (SEM) and tested electrically to verify the existence of a gap.

Appendix E – Schematic of the 1K cryostat.

Shutter for
1.5K pump

Vacuum
shutter

Cryostat
chamber

Vacuum
insulation
sleeve

Measurement
rod

Opening for
Helium

Needle
valve

Sample

Appendix F – Article: Measurement of the conductance of single conjugated molecules

Measurement of the conductance of single conjugated molecules

Tali Rosenblum[†a,b], Yoav Gordin[†a], Roman Krahne[a,c], Ilya Khivrich[a], Diana Mahalu[a], Veronica Frydman[d], Joseph Sperling[b], Amir Yacoby[a] and Israel Bar-Joseph[a*]

[a]*Department of Condensed Matter Physics, Weizmann Institute of Science, 76100 Rehovot, Israel*

[b]*Department of Organic Chemistry, Weizmann Institute of Science, 76100 Rehovot, Israel*

[c]*Present address: National Nanotechnology Labs of INFM, Lecce, Italy*

[d]*Chemical Research Support, Weizmann Institute of Science, 76100 Rehovot, Israel*

[†]*Equal contributors to this work*

[*]*israel.bar-joseph@weizmann.ac.il*

Electrical conduction through molecules depends critically on the delocalization of the molecular orbitals, and their weight on the metallic contacts. Thiolated (-SH) conjugated organic molecules are therefore often considered good candidates for molecular conductors[1,2]. In such molecules the orbitals are delocalized throughout the molecular backbone, with substantial weight on the sulfur-metal bonds[1-4]. However, their relatively small size, typically ~1 nm, calls for innovative approaches to realize a functioning single molecule device[5-11]. In this paper we report a new approach for contacting a single molecule and use it to study the effect of localizing groups within a conjugated molecule on the electrical conduction. Our method is based on synthesizing a dimer structure, consisting of two gold colloids connected by a di-thiolated short organic molecule[12,13], and electrostatically trapping it between two metal electrodes. We study the electrical conduction through three short organic molecules: A fully conjugated molecule, 4,4'-biphenyldithiol (BPD), Bis-(4-mercaptophenyl)-ether (BPE)[14] in which the conjugation is broken at the center by an oxygen atom, and

1,4-benzenedimethanethiol (BDMT), where the conjugation is broken near the contacts by a methylene group. We find that the oxygen in the BPE and the methylene groups in the BDMT suppress the electrical conduction relative to the BPD.

Various methods have been suggested and realized to form nanometer size gaps, including electron beam lithography with shadow mask evaporation[15] , mechanical break junctions[5-7], electromigration[8], and side etched quantum wells[16]. Molecules are then deposited on the thin gap, and it is assumed that electrical conductivity is obtained when a single molecule bridges the gap and conducts current. While impressive success in measuring the conductance of molecular junctions has been reported[5-7,9,10,17] serious problems are evident. The most notable are the uncertainty about the number of conducting molecules in the junction and the lack of information about the shape and structure of the metal contacts near the molecule. The dimer based contacting scheme presented here provides several advantages. (i) *Single* molecule devices can be fabricated with high certainty. (ii) The contacts to the molecule are well defined and can be characterized separately. (iii) It avoids the need for fabricating nanometer size gaps. (iv) It allows performing temperature dependent measurements of the molecular junction conductance over periods of hours and even days, regaining the original spectra after thermal cycling.

The dimer synthesis is performed by mixing a solution of dithiolated molecules with that of gold colloids, keeping their respective ratio below 1:10. The colloids were stabilized using the conventional citrate method[18]. In making the bridged dimers, the thiols on the bridging molecule displace citrate anions to form a stable Au-S bonds[19] (Fig. 1b, 1c). If more than one molecule binds to a certain colloid, trimers (Fig. 1d), tetramers (Fig. 1e) and higher oligomers can be formed. To ensure that most of the dimeric colloids are bridged by a single dithiolated molecule, the concentration of the latter (C_m) in the reaction mixture should be much smaller the concentration of the monomeric colloids (C_p). In that case, when the reaction is completed, the ratio R of dimers to single unbound colloids is expected to follow the relation $R \approx C_m/(C_p-2C_m)$. We measured R for different input concentrations of dithiolated molecules, keeping C_p fixed, and found that the above relation holds for $C_m{:}C_p$ ratios that are lower than 1:10.

Based on their relative mass, the dimeric colloids are separated from monomeric colloids and higher oligomers by centrifugation through glycerol or sucrose density

gradients. Each structure propagates as a different band along the centrifuged tube, and is easily distinguished because of its reddish color. Figure 1f shows a transmission electron microscope image at higher magnification of a dimer made of two 10-nm gold colloids connected by BDMT that is synthesized in this manner. The gap between the two colloids is readily seen, and its size is in good agreement with the size of the BDMT molecule, which is approximately 0.9 nm. To further establish the presence of a molecule in the dimer we conducted Raman scattering measurements on dimers with silver colloids[20]. A clear Raman spectrum was detected from a single dimer, with the characteristic temporal blinking of a single molecule.

We position the dimer in between two electrodes using the method of electrostatic trapping[15,16,21]. The gold electrodes are defined on a silicon substrate with a thin (25-100 nm) oxide layer using electron beam lithography. In most of our studies we use dimers with 30 nm diameter gold colloids. Hence, the electrodes are made with 40-50 nm separation, which is below the dimer size and larger than the single colloid diameter. The processed structures are first cleaned[22] and then inserted in a probe station where the electrostatic trapping is performed.

The success rate of the electrostatic trapping is relatively high, and reaches ~50% when the impedance of the dimer solution is high enough, such that the dipole-dipole interaction between the electrodes and the colloids is not screened. An analysis of the trapping events reveals that in 55% of the cases the gap is bridged by one colloid only. In 45% of the cases we get a dimer between the two electrodes (Fig. 2a): In 35% the conductivity is too low to determine the conductance features. We find in SEM imaging that the brightness of the gold colloids of these dimers is low, probably due to a poor conductivity between one of the colloids to the electrode [23]. In 10% of the trapping events we obtain high conductivity dimers. These are the samples that we refer to in this article: 11 BPD, 13 BPE and 15 BDMT devices.

Trapping single colloids in closely spaced electrodes (25-30 nm) allows us to study the current-voltage characteristics of the contacts. For the 30 nm gold colloids we find a Coulomb blockade staircase with a single electron charging energy of ~20-30 meV, and by applying a voltage to the substrate we can measure the diamond structure characteristic of a single electron transistor[24]. It is evident that a tunnel barrier with a typical resistance of ~10 MΩ is formed between the gold colloids and the electrodes, probably due to the ligands which stabilize the colloids in the solution.

The electrical transport measurements through the dimer structures are performed using an AC voltage with an amplitude of a few mV superimposed on a DC voltage, and the current as well as the differential conductance (dI/dV) are measured simultaneously. Figure 2b shows a comparison of the differential conductance of the three molecules at 4K. These are representative curves from more than ten devices of each of the molecular species that were studied. The BPD dimers clearly show a series of conductance peaks. These peaks cannot be attributed to charging of the gold colloids – their typical spacing is a few hundred mV, more than an order of magnitude larger than the gold colloids charging energy. In fact, in some cases we could resolve the Coulomb blockade oscillations superimposed on the large conduction peaks (see Fig. 2c). The oscillation period is very similar to that observed in a single colloid measurement (see comparison at the Supplementary Material section). We note that the conductance through a single trapped colloid is substantially higher than that of a dimer, typically by one to two orders of magnitude. Hence, the tunnel barriers between the metal electrodes and the gold colloids act as a small series resistance, carrying only a minute fraction of the applied voltage, while most of it drops on the molecule.

The BPE and BDMT dimers show remarkably different behaviors. It is clearly seen that the conduction through the dimers formed from these molecules turn on at much higher voltages (typically larger than 0.5V) and one cannot resolve any peak structure. The systematic difference between the three molecules further confirms that the measured differential conductance is of molecular origin. The apparent gap and exponential turn-on of the differential conductance in the case of the BPE and BDMT suggest that adding localizing groups interferes with the conjugated aromatic system and suppresses the overall conductance through the molecule. This assertion is nicely demonstrated when comparing the BPE with the BPD molecule, where the addition of an oxygen atom between the conjugated rings suppresses the conductance almost entirely below 1V. A similar effect takes place in the BDMT dimers where the methylene groups suppress the overlap of the molecular backbone orbitals with the contacts [25].

Focusing on the peak structure of the BPD dimers we find that while the main features of the conductance spectrum are highly reproducible, there are temporal fluctuations as well as variations between different devices. Figure 3a shows a compilation of 130 measurements of the conductance of one dimer taken over a period of a few hours. Strong temporal fluctuations in peak position, which could be as large as a few hundreds mV, are evident. We find that the conductance spectrum shifts rigidly, namely – all peaks at positive and negative voltages move to the same direction by approximately the same value. This is demonstrated in Fig. 3b, where we

shift all spectra such that their peaks at -0.2V coincide. It is seen that this operation causes all other peaks to be aligned as well. Such behavior is typical of electrostatically gated Coulomb blockaded systems with different input and exit capacitances [24]. Plotting the conductance in the V_{ds}-V_g plane one obtains a skewed diamonds structure (see Fig. 2 at the Supplementary Material section). It can be seen that under these conditions the conductance peaks at positive and negative drain-source bias indeed move rigidly upon application of a gate voltage. Since the gold colloids are very effective in screening the effect of remote potentials we conclude that charge movement in close vicinity to the molecule gives rise to the observed rigid shift of the spectrum. These temporal fluctuations can therefore be considered as evidence for gating of the molecule, which occurs randomly. We note that the temporal frequency of this random gating depends on the voltage sweep rate, dV/dt, and the voltage range of the measurement. It could be substantially minimized by working at low sweep rates and within a limited voltage range, such that stable and reproducible measurements can be conducted over hours.

The dimer structure allows us to conveniently perform temperature dependent measurements of the molecular junction conductance. We demonstrate this capability in Fig. 3c, which shows the behavior of the lowest voltage peak (~ -0.3 V in Fig. 3a) as the temperature is increased from 4K to 100K. It is evident that the peak broadens and decreases in height with increasing temperature, keeping the area approximately constant. The shift in peak position between the low and high temperatures measurements is due to gating which occurred during this long measurement. The broadening of the peak can be accounted for by the change in thermal distribution of the electrons in the leads. This mechanism is expected to broaden the peak by ~2kT (half width at half maximum).

Comparing the conductance of 10 BPD dimer-based devices shows that the variations between devices in the peaks position and their relative strengths cannot be explained only as a rigid shift. This is demonstrated in Fig. 4a, which compares the spectra of two BPD dimers. We can see that while the main features appear at approximately the same voltages, one cannot align the two spectra by a simple shift operation. We note also that there are differences in the value of the conductance between the various devices, which can be as large as an order of magnitude. To statistically quantify this variability we construct a histogram of peak positions (Fig. 4b). This is done by converting each spectrum to a set of peaks, each represented by a block of unit height, a width which is the full width at half maximum, and is centered around its maximum. A rigid shift of each spectrum was allowed to accommodate the temporal fluctuations. It is seen that the peak structure survives the averaging over many molecules, indicating that the variability in peak position is smaller than the peak spacing. The

peak positions determined from the histogram agree very well with measurements done on self assembled monolayers of BPD[26]. However, such agreement is lacking when comparing the measured spectra with recent calculations of molecular conduction[3,4]. In particular, the measured turn-on voltage is significantly lower than theoretically predicted. Moreover, the predicted conductance is several orders of magnitude higher than observed.

Methods

Colloidal gold nanoparticles with a diameter of 30 nm were prepared using a method described by Grabar et al.[18] with slight modifications. Briefly, a solution of "seed colloids" (2.6 nm) was prepared by adding 1.0 ml of 10mg/ml aqueous $HAuCl_4 \cdot 3H_2O$ to 100 ml of Milli-Q water while stirring. One min later, 1.0 ml of 10 mg/ml aqueous Na_3citrate was added followed, 1 min later, by 1.0 ml of freshly prepared 0.75 mg/ml $NaBH_4$ in water, and the mixture was stirred for 5 min. Larger colloids, 30 nm in diameter, were prepared by adding 0.2 ml of 10 mg/ml Na_3citrate and 130 µl of the Au "seed colloids" solution to 50 ml of boiling aqueous solution of $HAuCl_4 \cdot 3H_2O$ (0.1 mg/ml) while stirring. Refluxing was continued for 10 min, or until a change to a reddish color was observed. This procedure resulted in citrate-stabilized well-dispersed in water gold colloids[27] having a narrow size distribution[28] as confirmed by TEM. Gold colloid concentration was calculated based on the mean particle diameter measured by TEM and the weight of $HAuCl_4$ used in the reaction[19].

The dimer preparation consisted of several stages. First, the colloidal gold solution was concentrated. This was achieved by centrifuging the solution at 9.7×10^3 g for 5 min and discarding the supernatant. The precipitate was resuspended in 2.5 ml of 1 mM NaOH and centrifuged again as above, leaving about 0.4 ml of concentrated solution. The spacer dithiol-molecule was dissolved in 0.1 M NaOH and diluted with 1 mM NaOH to the desired concentration. This solution was mixed with an equal volume of the concentrated colloidal gold solution containing >10-fold molar excess of colloids and incubated for 24 hr at 4°C. The mixture (0.5 ml) was loaded on a 10%-75% glycerol gradient in water and centrifuged at 9,000 rpm for 10 min in a Beckman SW41 rotor. Fractions (0.5 ml) of the gradient were collected and characterized by TEM.

The electrodes are prepared on electron beam defined pattern, and consist of 20 nm of

Au on 10 nm of Ni that serves as an adhesion layer. The electrodes are cleaned in warm acetone and methanol for 5 min each, then placed in an ozone stripper for 8 min and finally stirred in ethanol for 10 min[22].

Electrostatic trapping is performed in a probe station; a 0.35 µL drop of the dimer solution (containing typically 45-55% dimers, 40-50% single colloids and a few percents of higher conjugates) is placed on the electrodes surface. Next an AC voltage of 800mV at 10MHz is applied between the electrodes for 1min. The sample is then cleaned in double distilled water, and blow dried in nitrogen. The devices are tested on the probe station, and the ones that show conductivity are bonded and measured at 4K. After the measurement the devices are imaged in a SEM to determine the type of colloidal structure that has been trapped.
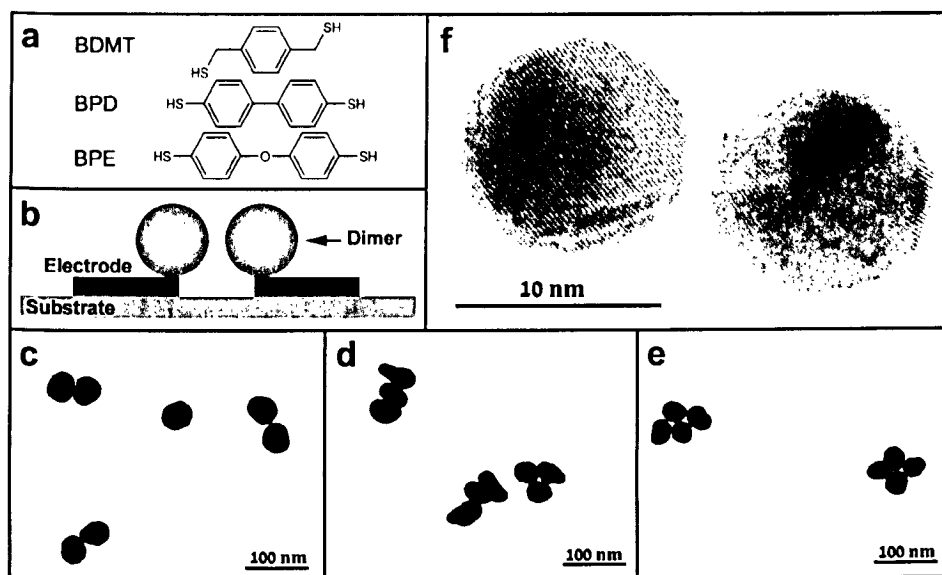
Figures:

Figure 1: The molecules and colloidal structures under study. a. The structure of the three molecules: 1,4-benzenedimethanethiol (BDMT), 4,4'-biphenyldithiol (BPD), and Bis-(4-mercaptophenyl)-ether (BPE). b. The dimer contacting scheme. c-e. TEM images of BDMT dimer, trimer and tetramer structures made of 50 nm gold colloids. f. TEM image of a BDMT dimer made of 10 nm gold colloids. The 1 nm separation between the two colloids corresponds approximately to the BDMT length (0.9 nm).
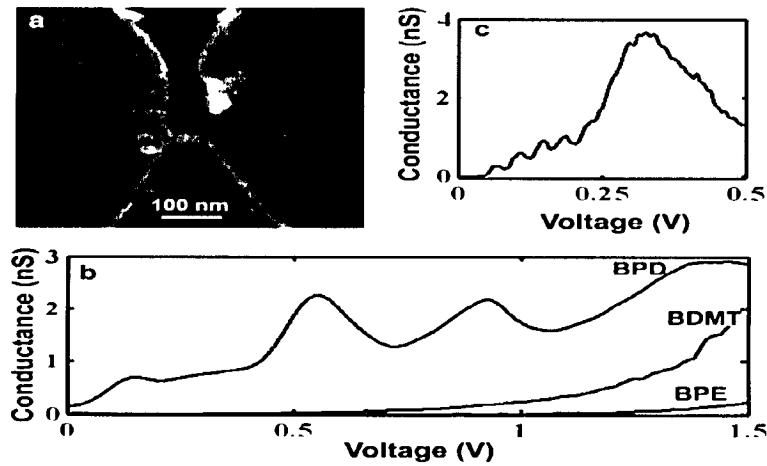
Figure 2: Low temperatures differential conductance spectra of dimers. **a.** SEM image of a dimer trapped between the two electrodes. **b.** The differential conductance as a function of voltage measured for BPD, BDMT and BPE dimers at 4.2 K. **c.** Coulomb blockade oscillations of the gold colloid which are superimposed on the conduction peak of the BPD measured at 4.2 K.
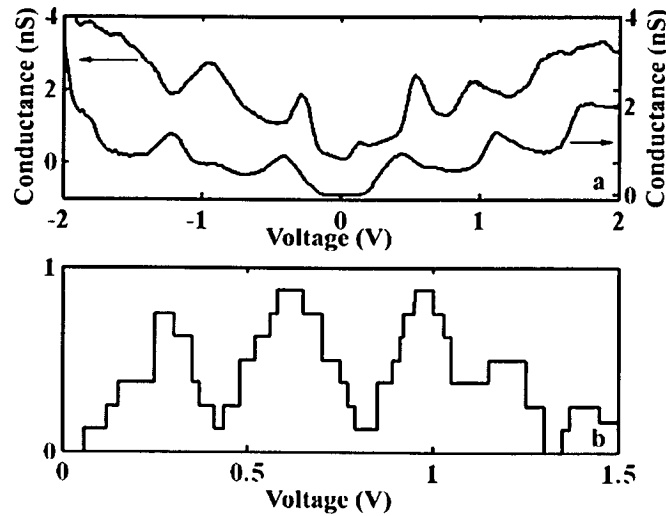

Figure 3: Temporal fluctuations and temperature dependence of the dimer conductance. **a.** A compilation of 130 measurements of the differential conductance spectrum of one BPD dimer, taken over a period of a few hours. The conductance values are represented by a color scale, which changes from blue (0 nS) to red (3 nS). **b.** The spectra of Fig. 3a shifted such that their peaks at -0.2 V coincide, thus demonstrating the rigid shift nature of the temporal fluctuations. **c.** The evolution of the lowest voltage conductance peak of a BPD dimer with temperature. A decrease in height and broadening of the peak with increasing temperature are observed.

Figure 4: The reproducibility of the conductance spectra measurements of different BPD dimers. **a.** Comparison of the differential conductance spectrum of two different BPD devices (The upper curve is shifted upwards for clarity). **b.** Histogram of the conductance peak positions collected from nine BPD devices. Each spectrum was converted to a set of peaks of unit height and a width which is the full width at half maximum. A rigid shift of the spectrum by up to 50 mV was allowed.
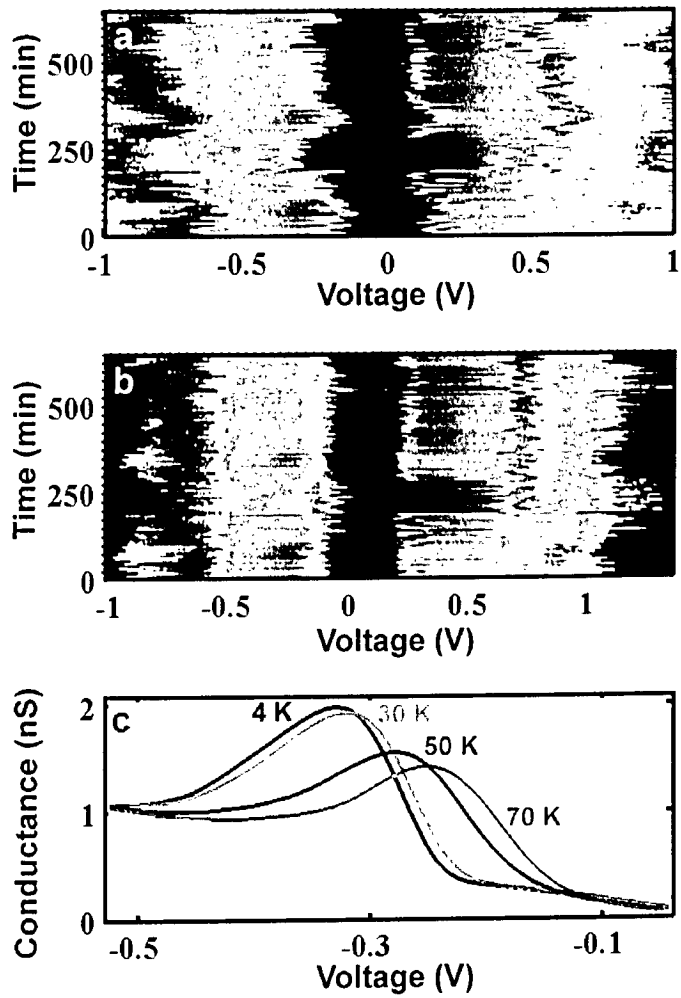
References:

1. Nitzan, A. & Ratner, M. A. Electron Transport in Molecular Wire Junctions. *Science* **300**, 1384-1389 (2003).

2. Joachim, C., Gimzewski, J. K. & Aviram, A. Electronics using hybrid-molecular and mono-molecular devices. *Nature* **408**, 541-548 (2000).

3. Xue, Y. & Ratner, M. A. Microscopic study of electrical transport through individual molecules with metallic contacts. I. Band lineup, voltage drop, and high-field transport. *Physical Review B (Condensed Matter and Materials Physics)* **68**, 115406-18 (2003).

4. Remacle, F. & Levine, R. D. Electrical transmission of molecular bridges. *Chemical Physics Letters* **383**, 537-543 (2004).

5. Reed, M. A., Zhou, C., Muller, C. J., Burgin, T. P. & Tour, J. M. Conductance of a Molecular Junction. *Science* **278**, 252-254 (1997).

6. Reichert, J. et al. Driving current through single organic molecules. *Physical Review Letters* **88** (2002).

7. Smit, R. H. M. et al. Measurement of the conductance of a hydrogen molecule. *Nature* **419**, 906-909 (2002).

8. Park, H., Lim, A. K. L., Alivisatos, A. P., Park, J. & McEuen, P. L. Fabrication of metallic electrodes with nanometer separation by electromigration. *Applied Physics Letters* **75**, 301-303 (1999).

9. Park, J. et al. Coulomb blockade and the Kondo effect in single-atom transistors. *Nature* **417**, 722-725 (2002).

10. Liang, W., Shores, M. P., Bockrath, M., Long, J. R. & Park, H. Kondo resonance in a single-molecule transistor. *Nature* **417**, 725-729 (2002).

11. Cui, X. D. et al. Reproducible Measurement of Single-Molecule Conductivity. *Science* **294**, 571-574 (2001).

12. Peng, X., Wilson, T. E., Alivisatos, A. P. & Schultz, P. G. Synthesis and Isolation of a Homodimer of Cadmium Selenide Nanocrystals. *Angewandte Chemie International Edition in English* **36**, 145-147 (1997).

13. Brousseau, L. C., III, Novak, J. P., Marinakos, S. M. & Feldheim, D. L. Assembly of phenylacetylene-bridged gold nanocluster dimers and trimers. *Advanced Materials (Weinheim, Germany)* **11**, 447-449 (1999).

14. Baron, A. L. & Blank, D. R. Synthesis and properties of some aromatic polythioethers. *Makromolekulare Chemie* **140**, 83-9 (1970).

15.   Bezryadin, A., Dekker, C. & Schmid, G. Electrostatic trapping of single conducting nanoparticles between nanoelectrodes. *Applied Physics Letters* 71, 1273-1275 (1997).

16.   Krahne, R. et al. Fabrication of nanoscale gaps in integrated circuits. *Applied Physics Letters* 81, 730-732 (2002).

17.   Park, H. et al. Nanomechanical oscillations in a single-C-60 transistor. *Nature* 407, 57-60 (2000).

18.   Grabar, K. C. et al. Two-dimensional arrays of colloidal gold particles: A flexible approach to macroscopic metal surfaces. *Langmuir* 12, 2353-2361 (1996).

19.   Weisbecker, C. S., Merritt, M. V. & Whitesides, G. M. Molecular Self-Assembly of Aliphatic Thiols on Gold Colloids. *Langmuir* 12, 3763-3772 (1996).

20.   Xu, H. X., Bjerneld, E. J., Kall, M. & Borjesson, L. Spectroscopy of single hemoglobin molecules by surface enhanced Raman scattering. *Physical Review Letters* 83, 4357-4360 (1999).

21.   Amlani, I., Rawlett, A. M., Nagahara, L. A. & Tsui, R. K. An approach to transport measurements of electronic molecules. *Applied Physics Letters* 80, 2761-2763 (2002).

22.   Ron, H., Matlis, S. & Rubinstein, I. Self-assembled monolayers on oxidized metals. 2. Gold surface oxidative pretreatment, monolayer properties, and depression formation. *Langmuir* 14, 1116-1121 (1998).

23.   Hazani, M. et al. DNA-mediated self-assembly of carbon nanotube-based electronic devices. *Chemical Physics Letters* 391, 389-392 (2004).

24.   Grabert, H., Devoret, M. H. & Editors. *Single Charge Tunneling: Coulomb Blockade Phenomena in Nanostructures. (Proceedings of a NATO Advanced Study Institute on Single Charge Tunneling, held March 5-15, 1991, in Les Houches, France.) [In: NATP ASI Ser., Ser. B., 1992; 294]* (1992).

25.   Xiao, X. Y., Xu, B. Q. & Tao, N. J. Measurement of single molecule conductance: Benzenedithiol and benzenedimethanethiol. *Nano Letters* 4, 267-271 (2004).

26.   Lee, J. O. et al. Absence of strong gate effects in electrical measurements on phenylene-based conjugated molecules. *Nano Letters* 3, 113-117 (2003).

27.   Zhu, T., Vasilev, K., Kreiter, M., Mittler, S. & Knoll, W. Surface modification

of citrate-reduced colloidal gold nanoparticles with 2-mercaptosuccinic acid. *Langmuir* **19**, 9518-9525 (2003).

28.   Handley, D. A. in *Colloidal Gold-Principles, Methods, and Applications* (ed. Hayat, M. A.) 13 (Academic Press, New York, 1989).

References

1. A. Aviram & M. A. Ratner, Chem. Phys. Lett., 29(2) (1974) 277.

2. C. Patoux, et al. J. Am. Chem. Soc. 120 (1998) 3717.

3. W. B. Davis, et al. Nature 396 (1998) 60.

4. S. Fraysse, C. Coudret, & J. P. Launay, Eur. J. Inorg. Chem. (2000) 1581.

5. C. Patoux, et al. Inorg. Chem. 36 (1997) 5037.

6. A. Nitzan J. Phys. Chem A 105 (2001) 2677-2679.

7. L. Segev et al. Phys. Rev. B 74 (2006) 165323.

8. A. Salomon, et al. Adv. Mat. 15(22) (2003) 1881-1890.

9. Y. Selzer and D. L. Allara Annu. Rev. Phys. Chem. 57 (2006) 593-623.

10. N.J. Tao Nature Nanotech. 1 (2006) 173-181.

11. Grabert, H., Devoret, M. H. Editors. *Single Charge Tunneling: Coulomb Blockade Phenomena in Nanostructures. (Proceedings of a NATO Advanced Study Institute on Single Charge Tunneling, held March 5-15, 1991, in Les Houches, France.) [In: NATP ASI Ser., Ser. B., 1992; 294]* (1992).

12. G. Cuniberti, et al. *Introducing molecular electronics*, Springer (2005).

13. R. Landauer, IBM J. Res. Dev. 1, 223 (1957).

14. R. M. Metzger, et al. J. Am. Chem. Soc. 119 (1997) 10455.

15. A. Nitzan & M. A. Ratner Science 300, 1384-1389 (2003).

16. S. Datta: *Electronic transport in mesoscopic systems* (Cambridge Univ. Press., New York,1996).

17. Y. Xue and M. A. Ratner, Phys. Rev. B 68, (2003) 115406.

18. Y. Xue and M. A. Ratner, Phys. Rev. B 69, (2004) 085403.

19. Y. Xue and M. A. Ratner, Phys. Rev. B 70, (2004) 081404(R).

20. S. M. Lindsay and M. A. Ratner Adv. Mat. 19, (2007) 23.

21. B. Muralidharan et al. ArXiv: cond-mat/0610244v1 (2006).

22. J. Reichert, et al Phys. Rev. Lett. 88 (17) (2002) 17 6804.

23. H. Park, et al. Nature 417 (2002) 722, W. Liang, et al. ibid 725.

24. J. Chen et al. Science 286 (1999) 1550.

25. D. Porath et al. Phys. Rev. B 56 (15) (1997) 9829.

26. C. Joachim and J. K. Gimzewski, Chem. Phys. Lett. 265 (1997) 353.

27. R. H. M. Smit et al. Nature 419, (2002) 906, D. Djukic et al. Phys. Rev. B 71, (2005) 161402.

28. K. Thygesen and K. W. Jacobsen, Phys. Rev. Lett. **94**, (2005) 036807.

29. D. Djukic *et al.* Phys. Rev. B **71**, (2005) 161402.

30. C. Patoux *et al.* Inorg. Chem 36 (1997) 3037.

31. C. E. D Chidsey Science 251 (1991) 919.

32. J. He *et al.* J. Am. Chem. Soc. 127 (2005) 1384.

33. B. Xu *et al.* Nano. Lett. 5 (2005) 1491.

34. D. Segal and A.Nitzan Chem. Phys. 268 (2001) 315.

35. Y. Selzer *et al.* Nano Lett. 5 (2005) 61-65.

36. C. Joachim *et al.* Phys. Rev. Lett. 74 (1995) 2102.

37. D. Porath, *et al.* Phys. Rev. B 56 (1997) 15 9829.

38. X. C. Cui *et al.* Science 294 (2001) 571.

39. M. Dorogi, *et al.* Phys. Rev. B 52 (1995) 12 9071.

40. Bezryadin, C. Dekker, J. Vac. Sci. Technol. B 15 (4) (1997) 793.

41. D. L. Klein, *et al.* Appl. Phys. Lett. 68 (18) (1996) 2574.

42. S. Kubatkin, *et al.* Nature 425 (2003) 698.

43. N. B. Zhitenev, H. Meng, & Z. Bao, Phys. Rev. Lett. 88 (22) (2002) 6801.

44. J. M. Van Ruitenbeek, *et al.* Rev. Sci. Inst. 67 (1) (1996) 108.

45. M. A. Reed, *et al.* Science 278 (1997) 252.

46. J Reichert, *et al.* Cond-Mat./ 0212272 v1 (2002).

47. H. Park, *et al.* App. Phys. Lett. 75 (2) (1999) 301.

48. A. Houck, *et al.* Nano Lett. 5 (9) (2005) 1685.

49. J. E. Grose, *et al.* Phys. Rev. B 71, (2005) 035306.

50. X. L. Li *et al.* Surface Science 573 (2004) 1-10 .

51. L. Venkataraman *et al.* Nature 442 (2006) 904.

52. F. Chen et al. Nano. Lett. 5 (2005) 503.

53. B. Xu *et al.* J. Am. Chem. Soc.127 (2005) 2386.

54. K.C. Grabar *et al.* Langmuir, 12 (10) (1996) 2353.

55. J. W. Slot, H. J. Geuze, European journal of cell biology 38, 87-93 (1985).

56. Moskovits, M. Rev. Mod. Phys. 57, 783-826 (1985).

57. E. J. Zeman and G. C. Schatz, J. Phys. Chem. 91 (1987) 634.

58. T. Dadosh Ph.D. thesis to be published.

59. Tang, X. and Schenider, T.W. *Langmuir, 12*, (1996) 5921.

60. R. Krahne *et al.* Appl. Phys. Lett. 81 (4) (2002) 730.

61. G. C. DeSalvo, W. F. Tseng, and J. Comas, J. Electrochem. Soc. 139, (1992) 831.

62. G. Maruccio *et al.* small 3 (7) (2007) 1184.

63. S. M. Luber *et al.* Nanotechnology **16** (2005) 1182.

64. H. A. Pohl Dielectrophoresis. Cambridge University Press, Cambridge UK 1978.

65. A. Bezryadin, C. Dekker & G. Schmid Appl. Phys. Lett. 71 (9) (1997) 1273.

66. A. Ramos *et al.* J. of Electrostatics 47 (1999) 71.

67. M. Hazani, *et al.* Chem. Phys. Lett. **391**, (2004) 389-392.

68. H. Ron, S. Matlis and I. Rubinstein, Langmuir **14**, (1998) 1116-1121.

69. S.K. Maiti, Physica B (2007), doi:10.1016/j.physb.2007.02.004

70. S. Wei *et al.* Phys. Rev. B 50 (1984) 14587.

71. J. K. Baria Chin. J. Phys. 42 (2004) 287.

72. L. L. Sohn, L. P. Kouwenhoven and G. Schön Editors proceedings of the Advanced Study Institute on *Mesoscopic Electron Transport.* (Kluwer 1997)

73. F. Grein J. of Mol. Struc. (Theochem) 624 (2003) 23.

74. J. O. Lee *et al. Nano Letters* **3**, (2003) 113.

75. F. Remacle & R. D. Levine, Chem. Phys. Lett. **383**, (2004) 537.

76. W. G. Van der wiel *et al.* Rev. Mod. Phys. 75, (2003) 1.

77. J. M. Taylor *et al.* Nature Physics 1 (2005) 177.

78. D. N. Weiss *et al.* App. Phys. Lett. **88**, (2006) 143507.

79. T. Junno *et al.* App. Phys. Lett. **80**, (2006) 667.

80. A. Guttman Masters thesis.

81. Baron, A.L. and Blank, D.R., *Makromol. Chem. 140*, (1970) 83-89.

82. Raasch, M.S. *J. Org. Chem. 44*, (1979) 2629-2632.

WEIZMANN INSTITUTE OF SCIENCE

Thesis for the degree
Doctor of Philosophy

חבור לשם קבלת התואר
דוקטור לפילוסופיה

By
Yoav Gordin

מאת
יואב גורדין

מדידת תכונות הולכה של מולקולות אורגניות בודדות בעזרת
ננו-חלקיקים מזהב

Measurement of the conductance properties of single
organic molecules using gold nanoparticles

Regular Format

Advisors
Prof. Israel Bar-Joseph
Prof. Amir Yacoby

מנחים
פרופ. ישראל בר-יוסף
פרופ. עמיר יעקבי

December 2006

דצמבר 2006

Submitted to the Scientific Council of the
Weizmann Institute of Science
Rehovot, Israel

מוגש למועצה המדעית של
מכון ויצמן למדע
רחובות, ישראל